INTERNATIONAL ATOMIC ENERGY AGENCY
INTERNATIONAL CENTRE FOR THEORETICAL PHYSICS
I.C.T.P., P.O. BOX 586, 34100 TRIESTE, ITALY, CABLE: CENTRATOM TRIESTE

H4.SMR/1058-11

WINTER COLLEGE ON OPTICS

9 - 27 February 1998

An Overview of Atomic Force Microscopy

B. Cappella

Institut de Physique Expérimentale, Université de Lausanne, Switzerland

MAIN BUILDING STRADA COSTIERA, 11 TEL. 2240111 TELEFAX 224163 TELEX 460392 ADRIATICO GUEST HOUSE VIA GRIGNANO, 9 TEL. 224241 TELEFAX 224531 TELEX 460449
MICROPROCESSOR LAB. VIA BEIRUT, 31 TEL. 2249911 TELEFAX 224600 TELEX 460392 GALILEO GUEST HOUSE VIA BEIRUT, 7 TEL. 2240311 TELEFAX 2240310 TELEX 460392

A. BEFORE ATOMIC FORCE MICROSCOPE.

The **resolution limit** of optical microscopes is $\lambda/2$, i.e. 0.2 μm for the visible light.
The first kind of microscope that got over this limit was the **Scanning Electron Microscope (SEM)**, that detects the electrons scattered from the surface of the sample, soon followed by the **Scanning Transmission Electron Microscope (STEM)**. The former has a resolution of about 100 nm, whereas the latter reaches 1 Å.
The **drawbacks** of these two microscopes are:

1. as the sample is "bombed" with electrons, it is dramatically damaged (biological samples above all);
2. they do not provide 3D images;
3. they need to work in Ultra High Vacuum (UHV);
4. they are very expensive.

In 1982 G. Binnig and H. Röhrer built the first **Scanning Tunnelling Microscope (STM)**, and were awarded of the Nobel Prize.
The STM exploits the tunnelling current between a sharp conductive tip (usually tungsten) and the sample surface. A voltage is applied between the tip and sample. STM can be operated in two ways: at constant height, i.e. keeping the tip always at the same height, or at constant current, i.e. keeping always the same tunnelling current between the tip and sample by means of a feedback loop that adjusts tip height. The scanning is carried out by a piezoelectric tube.
STM gives 3D images with a lateral resolution of 1 Å and a height resolution of 0.1 Å.

The **drawbacks** of STM are:

1. it works only with conductive samples (biological samples need a metallic coating);
2. it works preferentially in UHV or controlled atmosphere; anyway it cannot work under liquid.

B. ATOMIC FORCE MICROSCOPE.

In 1986 G. Binnig,C. Quate and C. Gerber invented the **Atomic Force Microscope (AFM).**
The heart of the AFM is a cantilever with a microfabricated tip that deflects when "touching" the sample surface.
Cantilever deflection may be collected in different ways, in order to reproduce sample topography.
The scanning is carried out by a piezoelectric tube.
A controller collects and processes data and drives the piezo scanner (fig. 1).
The controller contains of some A/D converters that receive data from the system of detection of cantilever deflections, some D/A converters that give signals to the piezo and an interface with a computer that stores data.

C. CANTILEVERS.

Early AFM employed cantilevers made with a tungsten STM tip bent at one end. Later on, cantilever began to be microfabricated on a chip. AFM **cantilevers** are usually in silicon or silicon nitride and may basically have two shapes: rectangular and "V"-shaped (fig. 2). The most important feature of AFM cantilevers is their **elastic constant**: if they are too soft, they deflect too much; if they are too rigid, they risk to damage the sample. For rectangular cantilevers the deflecting elastic constant k_l and the resonance frequency ω are given by:

$$k_l = \frac{1}{4} E \frac{wt^3}{L^3} \qquad \text{(C1)}$$

$$\omega = \sqrt{\frac{k_l}{m_{eff}}} \qquad \text{(C2)}$$

where E is the Young modulus ($1.5 \cdot 10^{11}$ Pa for the silicon nitride), w, t, L are given in fig. 2, and m_{eff} is an effective mass given by:

$$m_{eff} = m_t + 0.24 m_d \qquad \text{(C3)}$$

where m_d is the distributed mass and m_t the tip mass.
Also the torsion elastic constant is relevant:

$$k_t = -\frac{\beta G w t^3}{L} \qquad \text{(C4)}$$

where β is a numerical factor, G the stress modulus ($5.3 \cdot 10^{10}$ Pa for silicon nitride), and w, t, L are given in fig. 2.
In order to get the expressions of elastic constants of "V"-shaped cantilever computer simulations are often used.
Cantilevers back face (the face that is not to come in contact with the sample) is usually coated with a metallic (usually gold) thin layer in order to enhance reflectivity. This is necessary in liquids, where the reflectivity of silicon nitride is much reduced. This coating may bring some problems when the optical lever detection system is used (see below). In this case, a laser is focused on the cantilever that absorbs a part of the light; the silicon nitride layer and the metallic layer deform differently, causing parasitic deflections.

Also the **tip shape** is fundamental; nowadays, there are basically two kinds of tips: "normal" tips of pyramidal sphere-ended shape and with a radius of curvature of about 50 nm and conical "supertips" with an apex lesser than 20 nm that provides better resolutions (fig. 3).

D. METHODS OF DETECTION OF CANTILEVER DEFLECTIONS.

The methods employed to detect cantilever deflections are essentially three: **electronic tunnelling, interferometric** and **optical lever**.

electronic tunnelling

The tunnelling current between a metallic tip and the side of the cantilever that does not face the sample is revealed (fig. 4a): the cantilever has to be conductive or coated with a conductive material. This method, employed in the early AFM, gives several problems: first of all, the metallic tip next to the cantilever interacts with it and makes it deflect; furthermore it is not possible to work in liquids and, when working in air, contaminants store up between the cantilever and the tip.

optical lever

The optical lever method is the most used, as it is the most simple to carry out (fig. 4b). It consists in focusing a laser beam on the back side of the cantilever and in detecting the reflected beam by means of a position sensor, that is usually a quartered photodiode. The deflection and torsion signals are given in fig. 4b.

interferometric

By focusing a laser on the cantilever, the reflected beam interferes with a reference beam: deflections are revealed by the displacement of interference fringes.

E. PIEZOELECTRIC SCANNERS.

In order to acquire the cantilever deflection on several points of the sample, one need to move the cantilever on the sample, or, in other word it is necessary to **scan** the cantilever all over the sample.
Instead of moving the cantilever, it is better to move the sample, that is fixed on a transducer. Such a transducer must be able to do displacements of the order of Å with high precision. Hence **piezoelectric transducer** are the only ones suited for this task.
The piezoelectric effect is the capability of certain materials of developing a charge when under stress, whereas the inverse piezoelectric effect is the capability of deforming under an applied potential.
The piezoelectric actuator employed for atomic force microscopy are cylindrical tubes of different dimensions with two electrodes, one inside and the other outside, (usually nickel); the outer electrode is usually parted in four quadrants (fig. 5).
Usually the inner electrode is grounded. In order to obtain a deformation along the symmetry axis (Z axis) the same voltage is applied to the four quadrants; for displacements in the plane of the sample (XY plane), opposite voltages are applied between opposite quadrants and the inner electrode: one of the quadrants lengthens, the other shortens, resulting in a bending.
The extension ΔZ and the deflection ΔX of the tube are given by:

$$\Delta Z = -\frac{L}{w} d_{31} V \qquad \textbf{(2.1.3.3)}$$

$$\Delta X = -0.9 \frac{L^2}{rw} d_{31} V \qquad \textbf{(2.1.3.4)}$$

where 0.9 is a numerical factor, d_{31} is a parameter depending on the material, V is the voltage, and L, r and w are given in fig. 5.
The dependence of the displacement S on the voltage V is hysteretic. Piezo **hysteresis** is one of the major artefacts in AFM images: distances at the beginning of the scanning appear larger than distances at the end of the scanning: the images obtained scanning forward (sample from right to left) and backward (sample from left to right) are not identical. For this reason, in early AFM backward and forward images were shown separately.
Another non-linearity of piezotubes is **creep**. It is basically a delay effect depending on temperature: almost the entire displacement is done at the beginning, but a little fraction is done later with a logarithmic course.

Big efforts have been done in order to eliminate these non-linearities, with three different approaches:

1. *a posteriori* calculation of non-linear deformations due to hysteresis and creep;
2. independent measurement of piezo displacements with two different techniques: *capacitive technique* (the two plates of a capacitor are mounted one on the piezo and the other fixed on the support; displacements can be calculated on the basis of capacitance variations) and *interferometric technique* (the displacement of the interference fringes between a laser beam reflected by the piezo and a reference beam is measured);
3. use of electrostricitive transducers;
4. *charge-drive technique*: it consists in driving the piezo by controlling the charge instead of the potential; this may be achieved inserting a capacitor between the amplifier and the piezo.

F. OPERATION MODES

Also the AFM can be operated in constant height mode or constant deflection mode.

In **constant height** mode (fig. 6a) the sample moves only in the XY plane, always at the same distance from the chip supporting the cantilever; the cantilever deflects following sample topography; sample topography is drawn from deflections. This operation mode is the most immediate, but presents some drawbacks: if the sample has great differences in height, during the scanning the tip might be pressed onto the sample and might break.

In **constant deflection** mode the deflection of the cantilever, and hence the tip-sample force, is kept constant by means of a feedback loop.

Referring to fig. 6b, at the beginning the tip is approached to the sample till the force reaches a fixed reference value and the height h_1 is acquired. Then the sample is moved and, in general, the height h_2 differs from h_1: the cantilever deflects more or less than before. A feedback signal makes the sample move along the Z axis, withdrawing or approaching it, till the same value of force than before is reached.

If the microscope is operated in this way, the topography reconstruction is done by means of the correction signal of the feedback loop.

In principle, one can choose any repulsive or attractive force as reference force. As a matter of facts, a repulsive force (10^{-7}-10^{-9} N) is chosen, so that the tip and sample are always in contact during the scanning: the constant deflection operation mode with a repulsive reference force is called **contact** mode. There are two reasons for this choice:

1. the repulsive region of the force law is steeper than the attractive region (see fig. 7); hence, for the same variation in distance, the variation of force is bigger for repulsive forces (δF_r) than for attractive forces (δF_a), and hence there is a better vertical resolution;
2. repulsive interactions are short-ranged, whereas attractive interaction are long-ranged, hence, if the tip and sample are in contact, the effective tip surface interacting with the sample is smaller. The interaction is likely to be an ideal atom-atom interaction, and there is a better lateral resolution.

If the AFM is operated in contact mode, also the torsion of the cantilever can be detected. The torsion is due to lateral forces, that give information about the topography first derivative and the friction between the tip and sample.
The first line of fig. 8 shows schematically a line of a sample with a protrusion and a region of different friction; the second line shows the cantilever deflection: if the material with a different friction has the same height of the other, the deflection cannot reveal its presence. The third and fourth line shows the torsion of the cantilever in the forward and backward scanning.
Along the slope of the protrusion there is a lateral force that makes the cantilever bend, first in a direction and then in the other: the torsion depends on the slope of the sample and hence one can say that lateral force "sees" the topography derivative. The sign of the torsion is the same for the forward scanning and the backward scanning. On the contrary, the friction contribution to torsion changes in sign depending on the scanning direction. In order to separate the two contributions, it is sufficient to add and subtract the forward and backward scanning.
Fig. 9 gives an example of the different information drawn from a topographic image and a lateral force image.

Contact mode reaches the best resolution, but presents a rather important drawback: **dragging of soft samples**: if the sample is enough soft, the tip may deform it and/or drag away some parts (fig. 10).

In order to overcome such problems, a lot of alternative operation modes have been proposed; the most important are the **dynamic force mode**, and the **tapping mode**.
In both modes, the cantilever is supported by an extra piezo that can make it vibrate (fig. 11).
In **dynamic force mode** the cantilever is forced to oscillate ate the frequency ω_D next to the resonance frequency ω.
If the oscillation amplitude is small, the force exerted by the sample on the cantilever is given by:

$$F(z) \cong F(0) + \frac{\partial F}{\partial z} z = \left(k_l + \frac{\partial F}{\partial z} \right) z \qquad \textbf{(F1)}$$

where F(0) is the force on the still cantilever. The resonance frequency shifts from $\omega = \sqrt{k_l / m_{eff}}$ to ω', where

$$\omega' = \sqrt{\frac{k_l + \frac{\partial F}{\partial z}}{m_{eff}}} \qquad \textbf{(F2)}$$

The frequency shift may be kept constant by means of a feedback loop. As vibration amplitude must be small (5-30 nm), the tip may be trapped by water vapour layers on the surface.

Also in **tapping mode** (fig. 12) the cantilever is forced to oscillate next to resonance frequency, but the amplitude of oscillation is larger (20-100 nm) and the tip "taps" the surface at each oscillation. The oscillation amplitude changes depending on sample topography and may be kept constant by a feedback loop.
The tapping mode does not damage the sample, and is employed for soft sample, e.g. biological samples.

G. FORCE-DISTANCE CURVES.

An AFM **force-distance curve** is a plot of tip-sample forces vs. tip-sample distance.
In order to obtain such a plot, the sample is ramped along z axis and the cantilever deflection Δs_c is acquired. Tip-sample force is given by Hooke's law:

$$F=-k_c\Delta s_c \quad \text{(G1)}$$

The distance controlled during the measure is not the real tip-sample distance D, but the distance between sample surface and the rest position of the cantilever Z. These two distances differ because of cantilever deflection Δs_c and sample deformation Δs_s and are related by:

$$D=Z-(\Delta s_c+\Delta s_s) \quad \text{(G2)}$$

Therefore an AFM force-distance curve does not reproduce tip-sample interactions, but is the result of two contributions: the tip-sample interaction F(D) and the elastic force of the cantilever (G1).
Two characteristic features of force-distance curves can be noted: the discontinuities BB' and CC' and the difference between approach and withdrawal curve (fig. 13).
The difference in path between approach and withdrawal curves is usually called "**force-distance curve hysteresis**"; the two discontinuities are called "**jump-to contact**" in the approach curve (BB' in fig. 13) and "**jump-off-contact**" in the withdrawal curve (CC' in fig. 13). From B' onwards, i.e. going on pulling the sample against the cantilever, and from A to C along the withdrawal curve, the tip is in contact with the sample and the lines B'A and CA are called "**contact lines**". Before B in the approach curve and from C' onwards in the withdrawal curve the deflection is nearly zero and the horizontal lines here obtained are called "**zero lines**".
The **origin** of force-distance curves is usually put at the intersection between the prolongation of the zero line and the contact line of the approach curve.
Let us now give an **analytical expression** for force-distance curves. The cantilever-sample system can be described by means of a potential U_{tot} that is the sum of three potentials: $U_{cs}(D)$, $U_c(\Delta s_c)$ and $U_s(\Delta s_s)$. $U_{cs}(D)$ is the interaction potential between the tip and the sample, $U_c(\Delta s_c)$ is Hooke's elastic potential of the cantilever and $U_s(\Delta s_s)$ is the potential that describes sample deformation and is given, in a first approximation, by Hooke's law:

$$\begin{aligned} U_c(\Delta s_c) &= \frac{1}{2} k_c (\Delta s_c)^2 \\ U_s(\Delta s_s) &= \frac{1}{2} k_s (\Delta s_s)^2 \end{aligned} \qquad \text{(G3)}$$

where k_c and k_s are cantilever and sample elastic constants. Usually the interaction force can be written as:

$$F_{cs} = -\frac{\partial U_{cs}}{\partial D} = -\frac{C}{D^n} \qquad \text{(G4)}$$

where C and n depend on the specific forces acting between tip and sample.
The relation between Z and Δs_c can be obtained by forcing the system to be stationary:

$$\frac{\partial U_{tot}}{\partial(\Delta s_s)} = \frac{\partial U_{tot}}{\partial(\Delta s_c)} = 0 \qquad \text{(G5)}$$

As $\frac{\partial U_{cs}}{\partial(\Delta s_c)} = -\frac{\partial U_{cs}}{\partial(D)}$ (see eq. 2) we obtain:

$$k_c \Delta s_c = \frac{C}{(Z - \alpha \Delta s_c)^n} \qquad \text{(G6)}$$

where $\alpha=(1+k_c/k_s)$.
Eq. (G5) is the condition for U_{tot} to be stationary; however, if the system is in stable equilibrium, we must have $\frac{\partial^2 U_{tot}}{\partial(\Delta s_c)^2} > 0$, that is :

$$\frac{k_c}{\alpha} > nC \frac{1}{(Z - \alpha \Delta s_c)^{n+1}} \qquad \text{(G7)}$$

where k_c/α is the so called effective elastic constant. If the force gradient overcomes the effective elastic constant, the cantilever becomes unstable and "jumps" onto the surface. This discontinuity is the jump-to-contact. From equations (G6) and (G7) the cantilever deflection and the tip-sample distance at which jump-to-contact occurs can be determined:

$$\begin{cases} (\Delta s_c)_{jtc} = \sqrt[n+1]{\dfrac{C}{(n\alpha)^n k_c}} \\ D_{jtc} = \alpha n (\Delta s_c)_{jtc} \end{cases} \qquad \text{(G8)}$$

Information about **attractive forces** can be gained from the jump-to-contact: in particular, the maximum value of the attractive force equals the pull-on force, i.e. the product of jump-to-contact cantilever deflection and k_c. In order to relate attractive forces to tip and sample features the following issues are to be considered:
1. the forces acting between tip and sample;
2. the system geometry.

If the main force is the van der Waals force and the tip-sample system can be sketched as a sphere on a flat, the attractive force F_{attr} is given by:

$$F_{attr} = -\frac{AR}{6D^2} \tag{G9}$$

where A is the Hamaker constant and R the tip radius.
Another discontinuity occurs when, during withdrawal, the effective elastic constant overcomes the force gradient: this is the jump-off-contact. Jump-off-contact deflection and jump-off-contact distance are always greater respectively than jump-to-contact and jump-to-contact distance. This occurs for several reasons:
1. during the contact some adhesive bonds are created;
2. during the contact, the sample buckles and "wraps" around the tip, increasing the contact area: adhesion force thus depends also on indentation;
3. even without bonds or deformations, force-distance curves hysteresis contributes to make jump-off-contact larger than jump-to-contact;
4. meniscus force exerted by layers of liquid contaminants (chiefly water) acts against the pull-off.

The pull-off force, i.e. the product of jump-off-contact cantilever deflection and k_c, equals adhesion force, F_{ad}. In order to relate the tip and sample surface energies (γ_t and γ_s) and the adhesion force it is necessary to evaluate the deformations of the tip and the contact area. This can be done by means of different theories, i.e. Johnson-Kendall-Roberts (JKR), Derjaguin-Muller-Toporov (DMT) or Maugis. Considering the system as a sphere on a flat surface, according to DMT theory, the resulting **adhesion force** is:

$$F_{ad} = -4\pi R\sqrt{\gamma_t \gamma_c} \tag{G10}$$

Along contact lines (B'A and AC referring to fig. 13) Z and Δs_l are related by:

$$Z = \Delta s_l + \Delta s_c = \alpha \Delta s_l \tag{G11}$$

and if the sample is much stiffer than the cantilever, i.e. α=1, cantilever deflection equals sample movement. Thus the contact lines provide information

on sample **stiffness**.

G1. FORCE-DISTANCE CURVES IN AIR.

Fig. 14 shows a force-distance curve acquired on mica in air. Note that hysteresis is very large and that, while jump-to-contact is very small, jump-off contact is quite large.
Such a large adhesion is due to **meniscus force** exerted by a thin layer of water adsorbed onto the surface. This layer barely affects attractive forces, while, due to the high surface energy of water, it prevents the tip from pulling off from the surface. Similar curves, with pull-off forces of nearly 30 nN and pull-off distances of nearly 500 nm, are obtained both on silicon and graphite. Meniscus force overcomes all other forces and so, in particular, they mask van der Waals force. In order to measure van der Waals force, meniscus force must be eliminated, either by removing the water layer by working in a low humidity environment (such as dry nitrogen), or by dipping both sample and tip in a liquid environment.

G2. FORCE-DISTANCE CURVES IN WATER AND OTHER LIQUIDS: VAN DER WAALS FORCE.

Immersing both sample and tip in liquid is a way to remove meniscus force and measure van der Waals force and other interactions weaker than meniscus force.
Fig. 15 shows a curve acquired on mica in water. There, both attractive and adhesion forces become nearly ten times smaller than in air and, as meniscus has been removed, the **van der Waals force** makes the greatest contribution to adhesion. Pull-off distance is also reduced by a factor of ten. Note the attractive force just before the jump-to contact; it follows an inverse square law. This is a feature typical of the van der Waals force between a spherical and a flat surface.

Some liquids, such as formamide or glycerol, unlike the majority of liquids, have **repulsive van der Waals forces**, while some others, such as water, H_2O_2 and glycol, present a specific distance at which van der Waals force turns from attractive to repulsive. Van der Waals force is in fact the result of two contributions: the entropic term, that is repulsive, and the dispersion one, that is usually attractive. Due to the retardation effect, at distances of nearly 100 nm, the dispersion term follows an inverse cube law (in the case of forces between a sphere and a flat surface), while the entropic term keeps following an inverse square law. Thus, at small distances, the dispersion term may overcome the entropic one and the resulting van der Waals force is attractive; as distance increases, the retarded dispersion term may become smaller than the entropic one and the van der Waals force becomes repulsive. For some liquids, the

dispersion term is also repulsive and the force is repulsive at any distance. This is the case of **formamide**.
In fig. 16 a force-distance curve acquired on mica in formamide is shown: before the jump-to-contact and after the jump-off-contact, the force follows a D^{-2} law and is repulsive.

G3. DOUBLE LAYER FORCE.

Unfortunately, van der Waals force are not the unique forces in water. In the approach curve, just before the attractive van der Waals region, there is a repulsive force that raises the curve over the zero line (fig. 15). This is the **double-layer force**, due to the charging of both sample and tip surfaces in liquids. This charging can occur either adsorption of ions from the solution onto the surface or for dissociation of functional groups on the surface.
Without discussing the straight derivation of equations describing this force, let us say that the surface charge creates a counterion distribution in the liquid gap between the surfaces (fig. 17); as the two surfaces approach, the squeezing of the liquid phase counteracts the configurational entropy that causes counterions to stay apart from each other. The resulting repulsive force in the approach curve is given by:

$$F_{d.l.} = \frac{2\pi R}{\varepsilon_l \varepsilon_0 k}\left[\left(\sigma_T^2 + \sigma_S^2\right)e^{-2kD} + 2\sigma_T\sigma_S e^{-kD}\right] \qquad \text{(G3.1)}$$

where D is the distance between the surfaces, σ_T and σ_S the surface charge densities of tip and sample respectively, ε_l the dielectric constant of the liquid, R the tip radius and $1/\kappa$ is the so-called **Debye length** given by:

$$\kappa = \sqrt{\sum_i \frac{\rho_i e^2 z_i^2}{\varepsilon_l \varepsilon_0 kT}} \qquad \text{(G3.2)}$$

where ρ_i is the concentration of the i-th electrolyte, $z_i e$ its charge, and T the temperature.
Thus double-layer force depends both on surface charge and on electrolyte concentrations in the solution.
Fig. 18 shows force-distance curves on mica in solutions with **different KCl concentrations**. Increasing the concentration up to 0.1 M, three changes occur:
1. the repulsive force becomes smaller and smaller;
2. its decay length diminishes;
3. the van der Waals force appears.
At 0.1 M KCl concentration, the force-distance curve resembles the one in deionized water (fig. 15). As deionized water is a solution 10^{-7} M in both H_3O^+

and OH^-, it should show the highest double-layer force: so it is, but, as the decay length tends to infinity, the exponential force approaches a horizontal line and the origin of the forces is unknown.
Further increasing the concentration, another repulsive force with exponential decay appears. This force is the hydration force, arising from electrolyte ions opposing to being deprived of their water solvation shell.
A similar set of curves can be obtained with other electrolytes. Using a 2:1 electrolyte such as $MgCl_2$, at the same concentration, the force and the decay length become smaller: this is due to the dependence of the Debye length on ionic force (fig. 19).
In order to study the dependence of double layer force on **surface charging**, force-distance curves may be acquired on a sample whose surface charging depends on the pH of the water solution. This is the case of stearic acid (fig. 20), whose pK is 8.
This means that, at pH less than 8, sample surface is uncharged, there is no double-layer force and there is a jump-to-contact due to van der Waals force; at pH 8.1 the surface begins charging and double-layer force counterbalances van der Waals force, so that there is no jump-to-contact; finally, at pH greater than 8, there is a considerable double-layer force with its characteristic exponential decay.

G4. HYDROPHOBIC FORCE AND BRIDGING FORCE.

In water, another kind of force can be seen: the **hydrophobic force** (fig. 8). If the sample surface is hydrophobic and is dipped in water, after the tip has contacted the sample, sample molecules "prefer" to be in contact with the tip rather than with water. Thus, when the sample is retracted, these molecules exert a force opposite to the tip movement. This force results in withdrawal curves with a "slide-off-contact", i.e. a gradual and continuous pull-off, instead of a jump-off-contact, i.e. a discontinuity.
Examples of these curves can be obtained with gold, that, like all other metals, when exposed to air, becomes hydrophobic due to the adsorption of a thin layer of alkanes.
These "slide-off" curves become "jump-off" curves if gold is dipped into ethanol or cleaned with ethanol, which dissolves the alkane layer.
The hydrophobic gives a pull-off force dramatically bigger than that due van der Waals force (8nN vs. 1-2 nN); this force can be increased employing a gold tip, because the interacting hydrophobic forces are now two (fig. 21).
The same force can be observed on stearic acid and causes a peculiar phenomenon: the formation of **bridging necks** between the tip and the sample. When withdrawing the tip, these necks cause a series of detachments after the

jump-off-contact (fig. 22). Such detachments have neither a preferential breaking force, nor breaking length, nor elastic constant.

G5. SOLVATION FORCE.

Octametylcyclotetrasiloxane (OMCTS) is a liquid with an approximately spherical molecule, whose radius has been estimated by two different authors at 0.76 nm and 0.9 nm respectively. Thus, OMCTS is particularly suitable to measure **solvation force**. This is a force caused by the ordering of liquid molecules between two liquid-solid interfaces (fig. 23).
The closer the tip approaches to the sample, the more the liquid molecules increase their ordering; before contacting the surface, the tip encounters some layers of liquid molecules and must exert a certain force to eliminate them. Thus the pressure follows the density of the solvent molecules and has a damped sinusoidal shape:

$$P(D) \cong -kT\rho_l(\infty)\cos\frac{2\pi D}{\sigma}e^{-D/\delta} \qquad \text{(G5.1)}$$

where D is the distance between solid surfaces, $\rho_l(\infty)$ is the limit of the liquid's density for D going to infinity, δ is the liquid molecule diameter and T the temperature. This damped sinusoid is superimposed on the van der Waals force and overcomes it one when $A<10^{-21}$ J.
Due to the dependence of AFM force-distance curves on cantilever elastic constant, oscillations results in a series of jumps followed by a repulsive region.
Fig. 23 shows force-distance curves on graphite in OMCTS, with a series of five jumps due to solvation force. The measured value of the force (0.1 nN) is of the same order of that predicted by eq. (16).
Solvation force cannot be measured in all liquids: some of them have a Hamaker constant too high and the van der Waals force "hides" the solvation force; some others have a molecular radius too small or, what is perhaps most important, the shape of their molecule does not allow a regular layering at interfaces. Anyway, solvation force has been measured not only in OMCTS, but also in dodecanol and in water.

G6. FUNCTIONALIZED TIPS AND SPECIFIC FORCES.

The tip of an AFM can be covered with almost any kind of molecules, in order to study the interaction between two particular molecules, one on the tip and one on the sample. The most used **functionalizations** are metals, hydrophobic molecules and biological molecules. Biological molecules can interact specifically with other molecules.

Figure 25 shows a typical withdrawal curve with **specific adhesion** between Olfactory Binding Protein (OBP) molecules and its antibody. After a first slide-off-contact of about 300 pN due to aspecific adhesion, mainly van der Waals force, tip and sample should detach, but OBP and antibody molecules are still bound by long and flexible bonds which are stretched along the subsequent attractive surge until the force reaches a rupture value. The discontinuity of about 1 nN at a distance of 225 nm marks the detachment due to the rupture of the specific bonds between OBP and its antibody. As the antibody molecules bound to OBP molecules may be located at different points on the tip, and hence detach at different distances, several curves present multiple detachments. It is important to point out that the detection of such specific bonds is based on the unique shape of the attractive regions and not on the strength of the adhesion force. In some cases the jump-off-contact and the specific detachment may partially or completely overlap, depending on the rupture distance; it is possible to discriminate between the two kinds of jumps by means of the dependence of the attractive region on the distance, that is quite linear for the jump-off-contact and in most cases non-linear for the specific detachment.
This forces have the same shape of bridging forces, but the rupture force is quantized, i.e. each detachment corresponds to a multiple of an elementary force that is the rupture force between a single protein-antibody couple. Hystograms of these forces thus present a series of peaks.

STUDYING INTERACTION SPATIAL VARIATION.

Fig. 27 shows withdrawal force-distance curves on the points of the middle line of this area; the inset shows the lateral force image previously obtained by means of a contact acquisition: first and last curves of this line are on Fluoresceine Isothyocianate (FITC), while central curves are on silicon. Both the pull-off distance and the jump-off-contact are smaller on FITC than on silicon. It is then possible to discriminate materials by means of sequential acquisition of force-distance curves.
Fig. 28 shows a series of four images, called **force slices**, obtained collecting the deflection of the cantilever at a fixed distance from the point of maximum load all over the points of the scanned area. These force slices have been taken at different distances (250, 300, 350 and 440 nm) near the jump-off-contact. Let us now consider force-slices near jump-off-contact.
In the first force-slice, at some FITC points, the tip has already pulled off the sample, while, on silicon, it still adheres to the surface. When the distance increases, the tip pulls off from more and more FITC points, but keeps on adhering to silicon; in the last force-slice shown, FITC regions are completely white and silicon region is completely black. Note that the last image looks like an "on-off" image.

The widely different behaviour of FITC and silicon in these force-slices suggests that Si_3N_4 tip adhesion forces with FITC are weaker than with silicon. From force-distance curves, the average pull-off force on FITC is 16 nN, while it is 22 nN on silicon.
Since measurements were done in air, water meniscus force is the greatest contribution to pull-off forces; hence, such differences in forces are due both to a different behaviour of the aqueous layer between FITC and silicon and to the different surface energies of the two materials.

Another approach to study interactions spatial variation is calculating interesting parameters (such as compliance, jump-to-contact and jump-off-contact) from all the curves and plot them, drawing a **map**. Figs. 30 and 31 show maps for the compliance, the jump-off-contact, the jump-off-contact distance and the adhesion of the FITC sample.

The same kind of images can be obtained in water, where adhesion forces are really due to van der Waals forces but, as we have already seen, are much smaller. This makes the detection more difficult. In order to enhance the contrast, biological samples can be put on hydrophobic substrates, that have a much bigger adhesion force.

ATOMIC FORCE MICROSCOPE

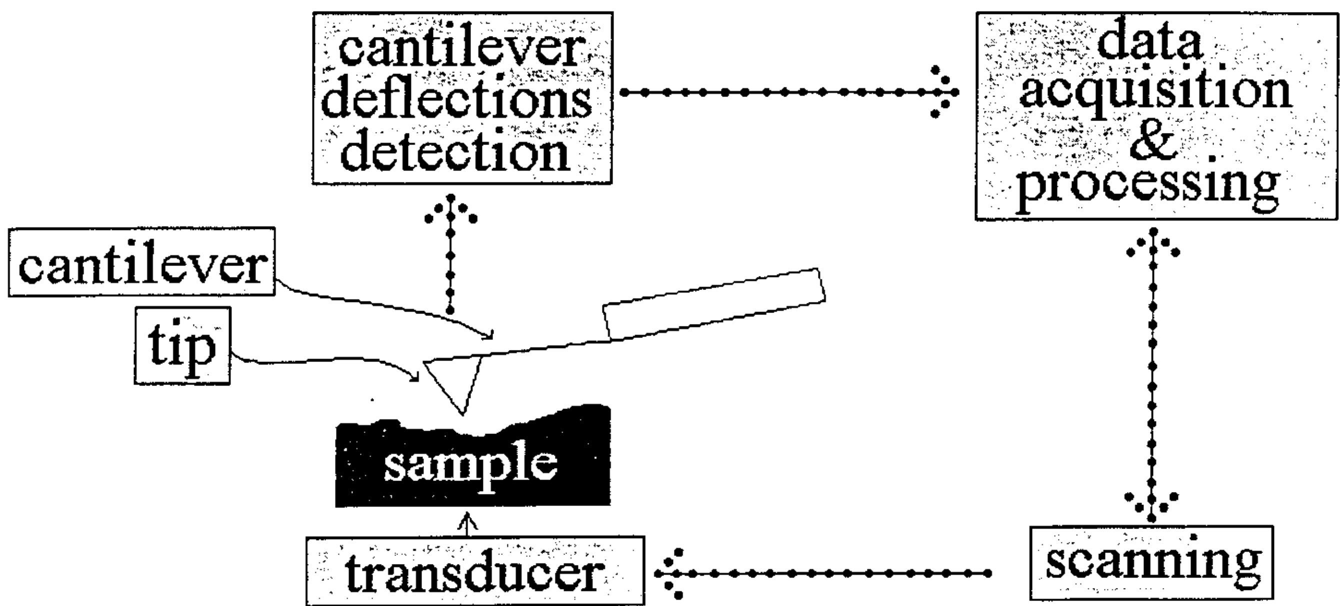

fig. 1

CANTILEVERS

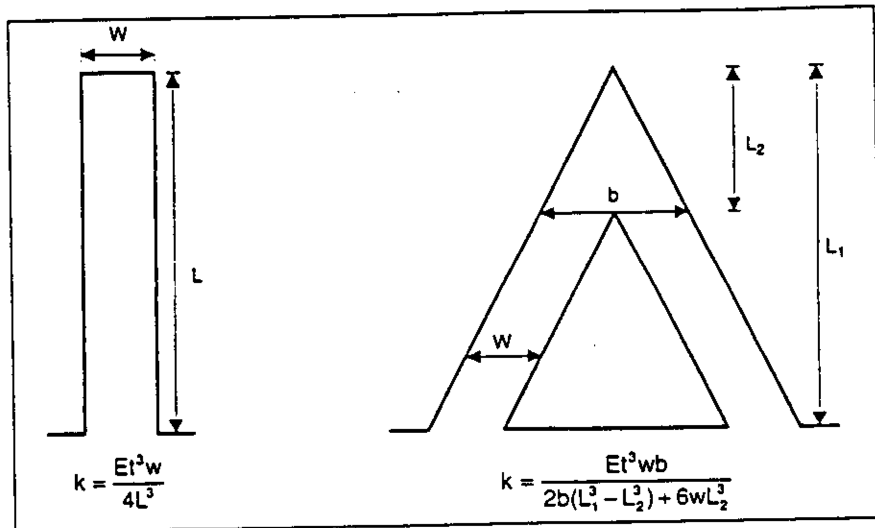

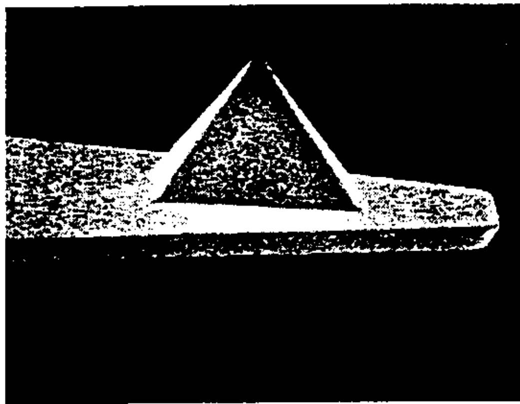

Close-up view of a pyramidal tip.

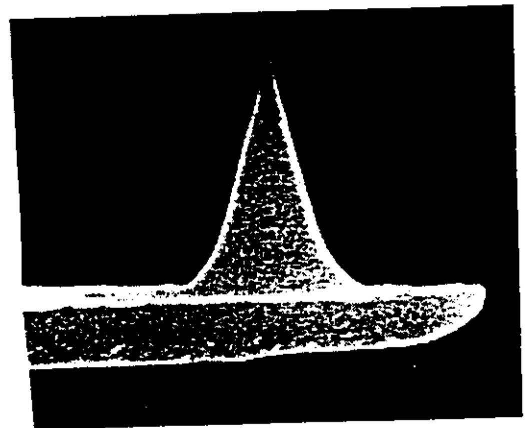

Close-up view of a silicon conical tip.

MATERIALS: Si, Si_3N_4
COATING: Au, Al

fig.2

EFFECT OF TIP SHAPE

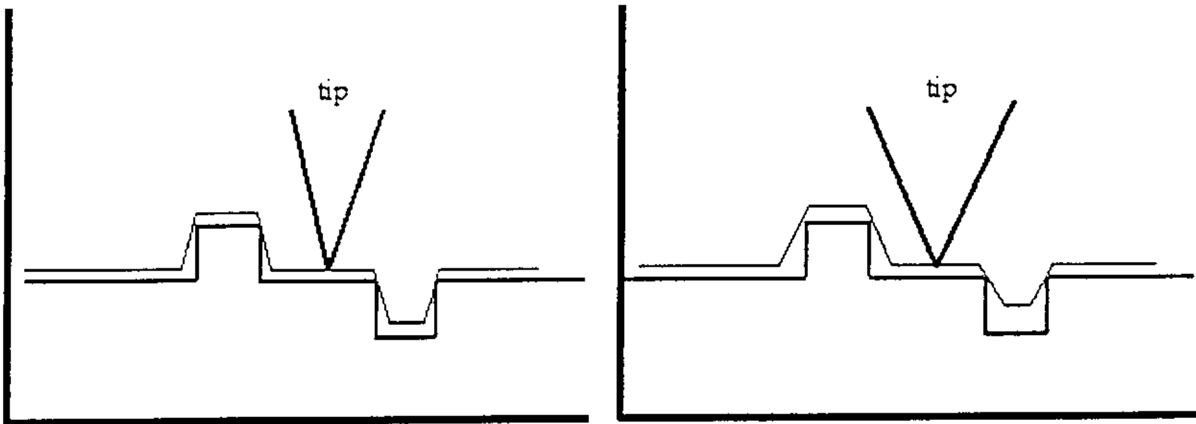

SHARP TIP

LARGER TIP

fig. 3

How can cantilever deflections be detected?

TUNNELING TIP

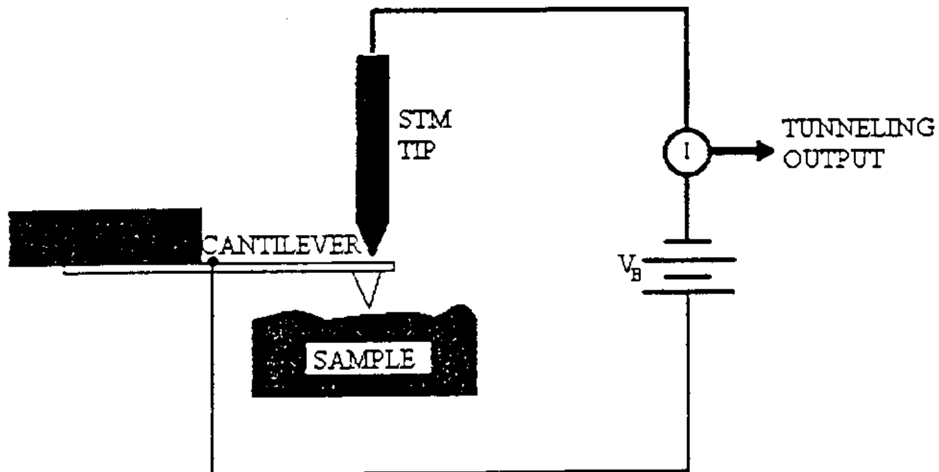

fig. 4a

OPTICAL LEVER

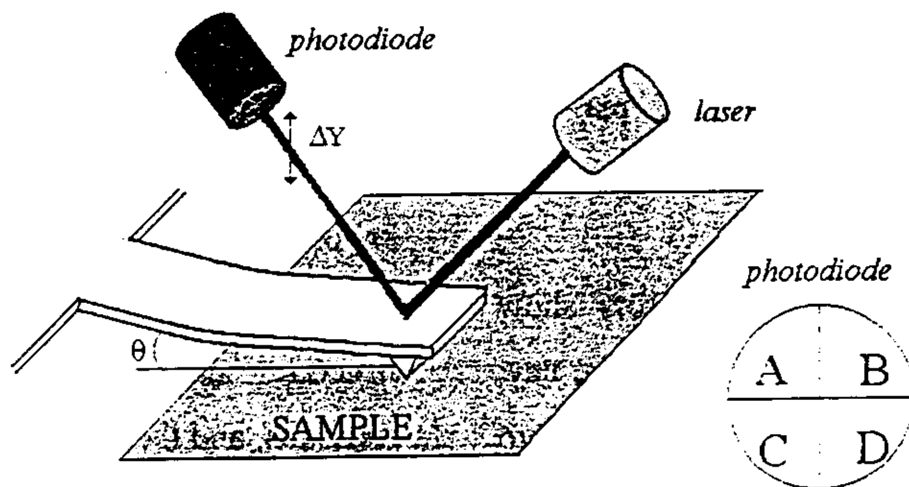

$$\text{DEFLECTION} = \frac{(A+B)-(C+D)}{A+B+C+D}$$

$$\text{TORSION} = \frac{(A+C)-(B+D)}{A+B+C+D}$$

fig. 4b

PIEZO SCANNERS

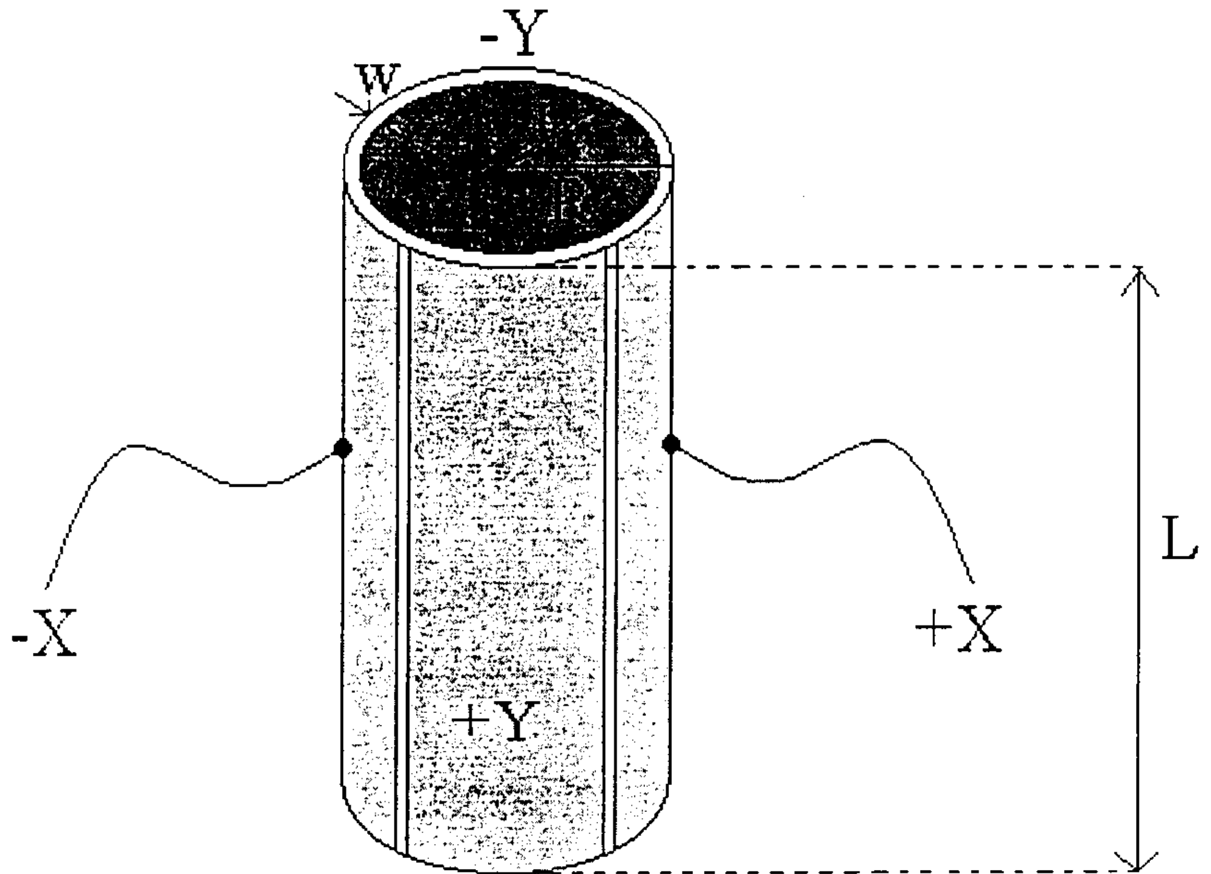

$$\Delta Z = -\frac{L}{w} d_{31} V$$

$$\Delta X = -0.9 \frac{L^2}{rw} d_{31} V$$

fig. 5

CONSTANT HEIGHT

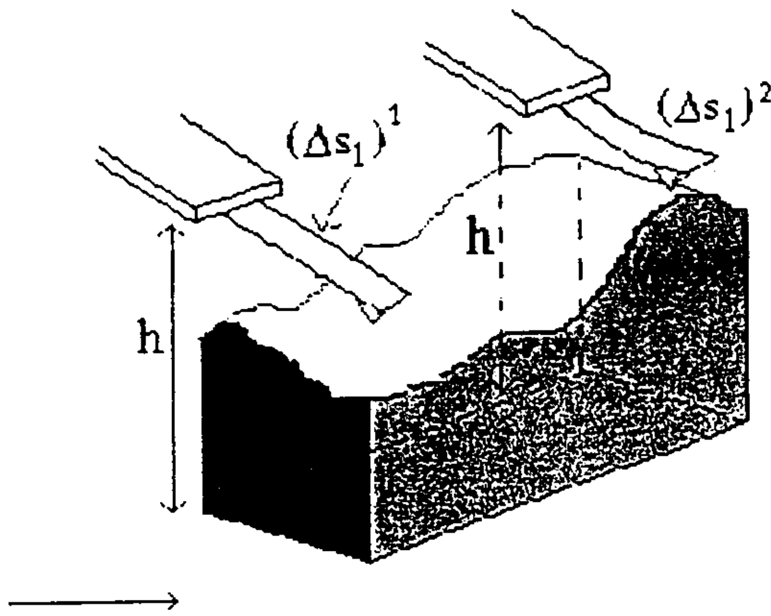

fig. 6a

CONSTANT DEFLECTION

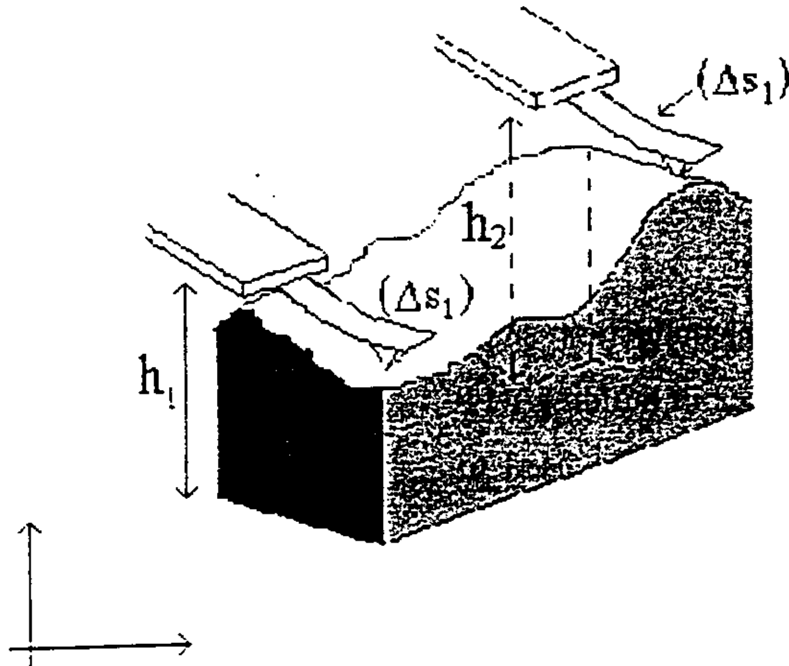

fig. 6b

How can a microsized tip "see" atoms?

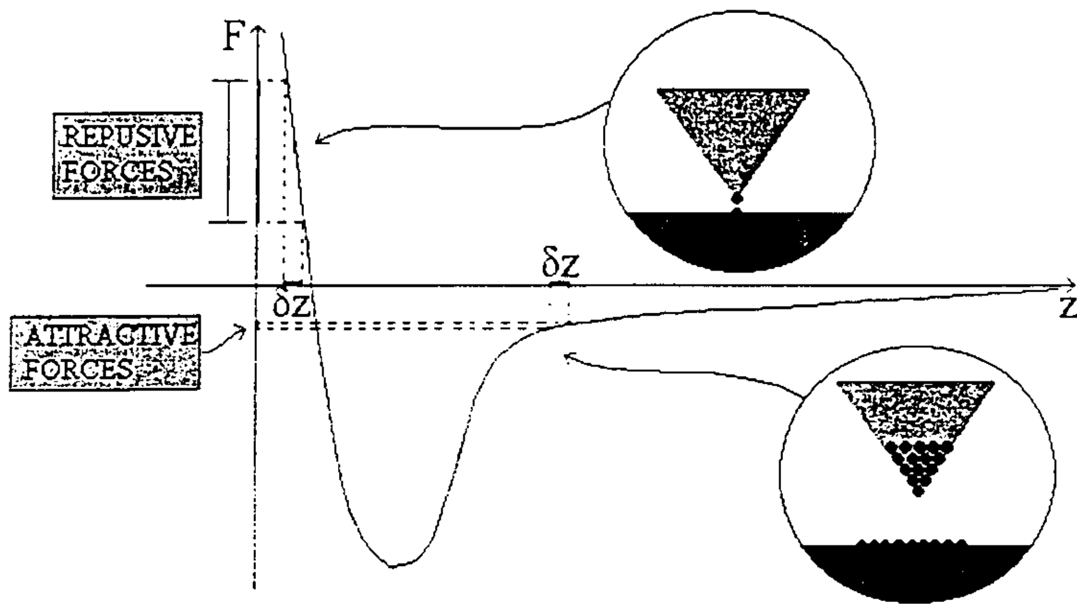

fig. 7

LATERAL FORCE IMAGES

-first derivative effect
-friction effect

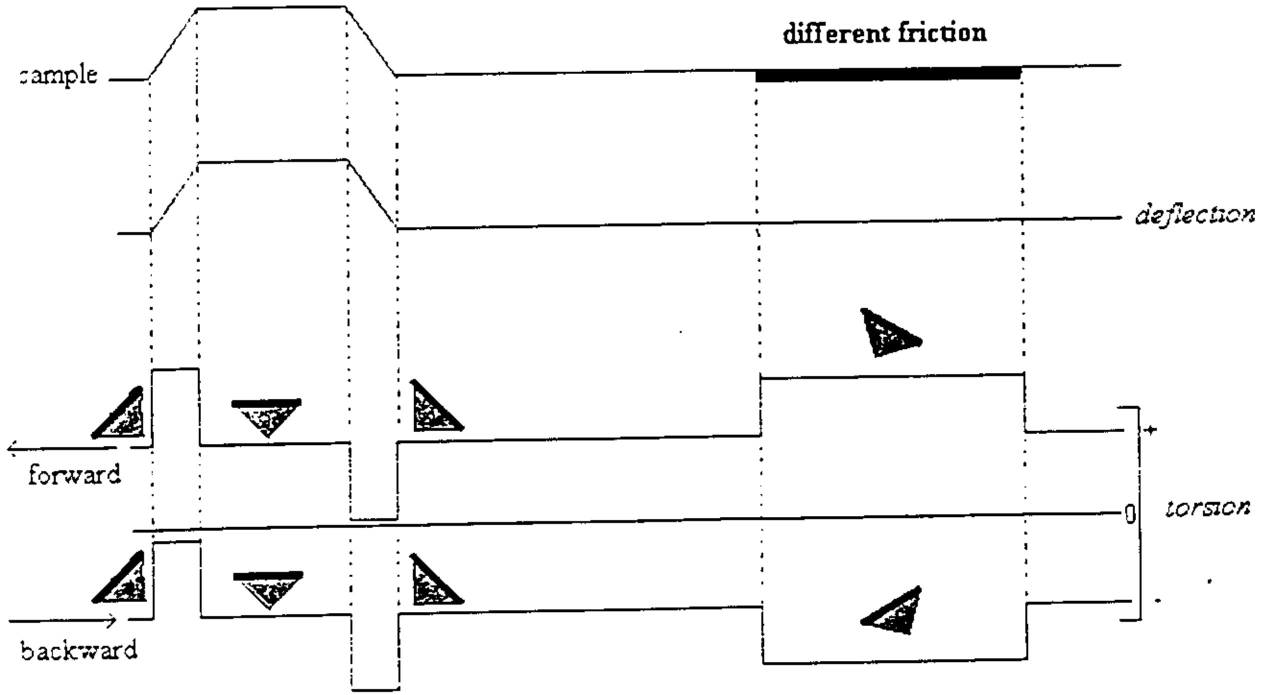

fig. 8

PHOSPHATIDILCOLINE DENDRITES on SILICON

TOPOGRAPHY

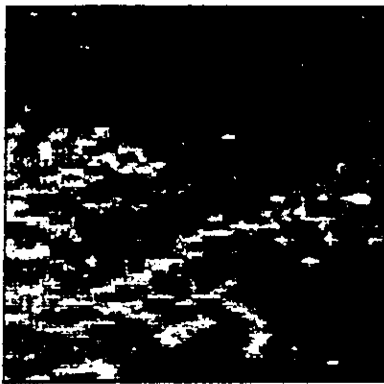

forward

backward

FRICTION

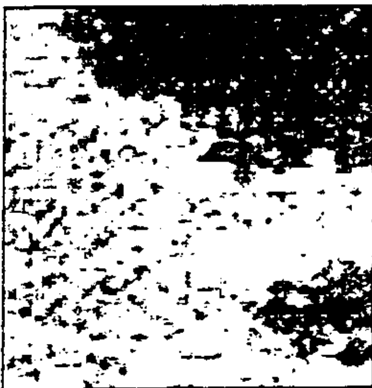

forward

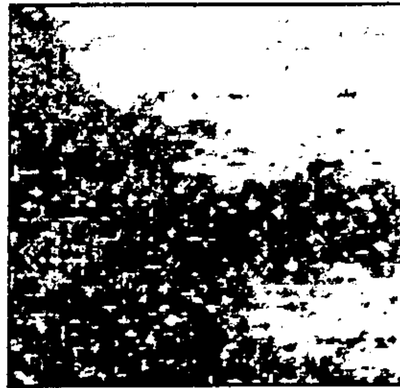

backward

Fig. 9

CONTACT MODE MAY DAMAGE SOFT SURFACES

POLYSTYRENE LATEX PARTICLES ON MICA IN WATER.

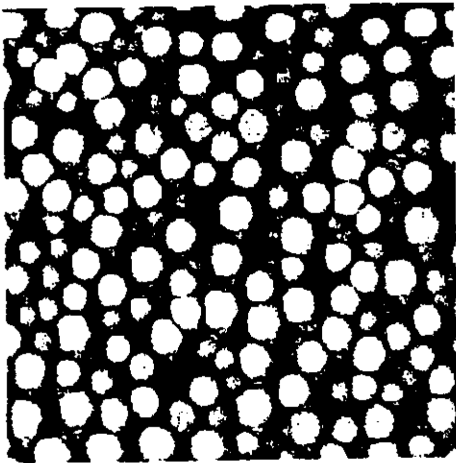

Tapping Mode image.

3 µm scan.

Contact Mode image.

3 µm scan.

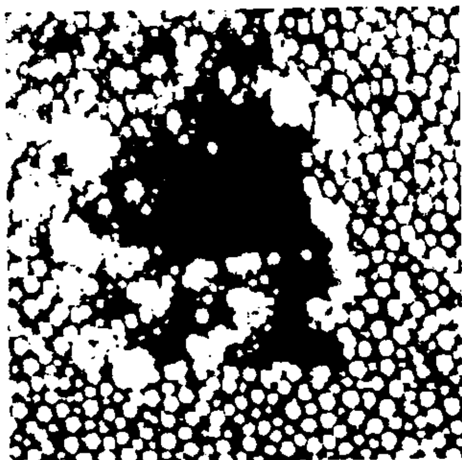

TappingMode image
<u>after a contact mode scan.</u>

7 µm scan.

fig.10

BEHIND CONTACT MODE

CONTACT MODE ⇒ cantilever quasi-static bending

non-contact, **tapping** or *intermittent contact* mode

the cantilever is excited by an extra piezo

changes in the oscillation
frequency, **amplitude**, or *phase* are recorded

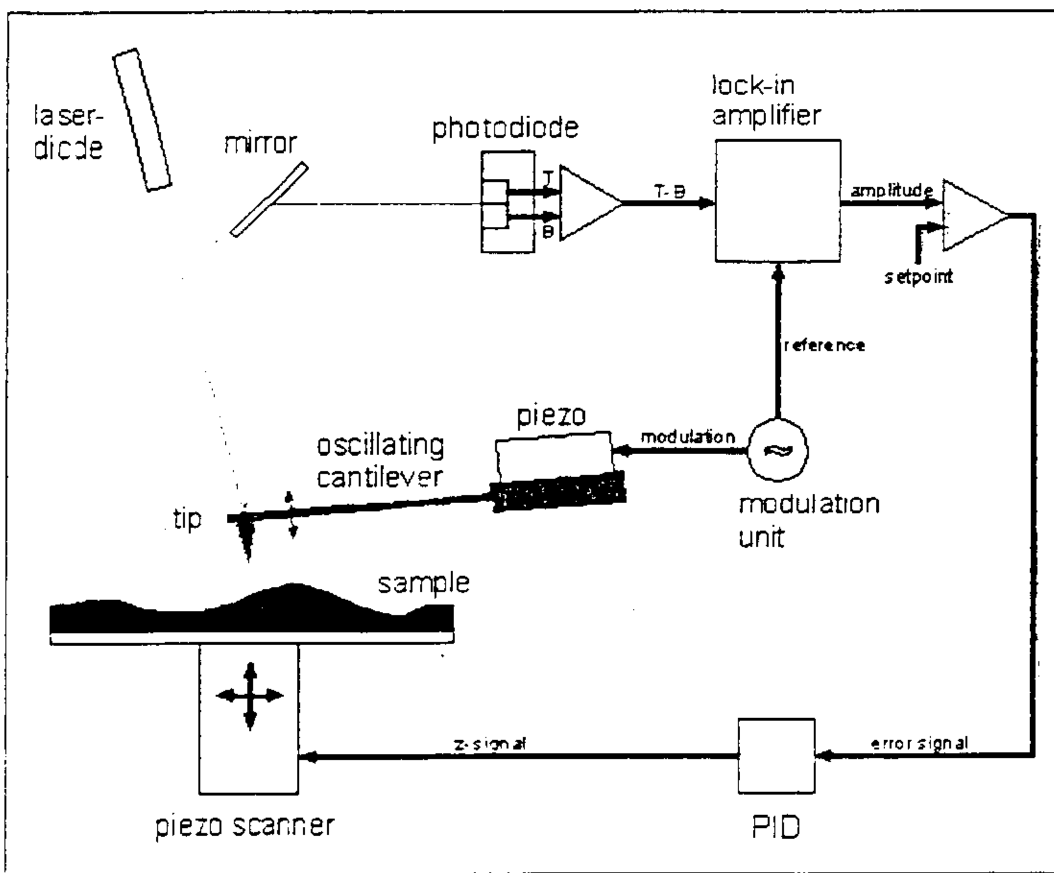

fig. 11

TAPPING MODE

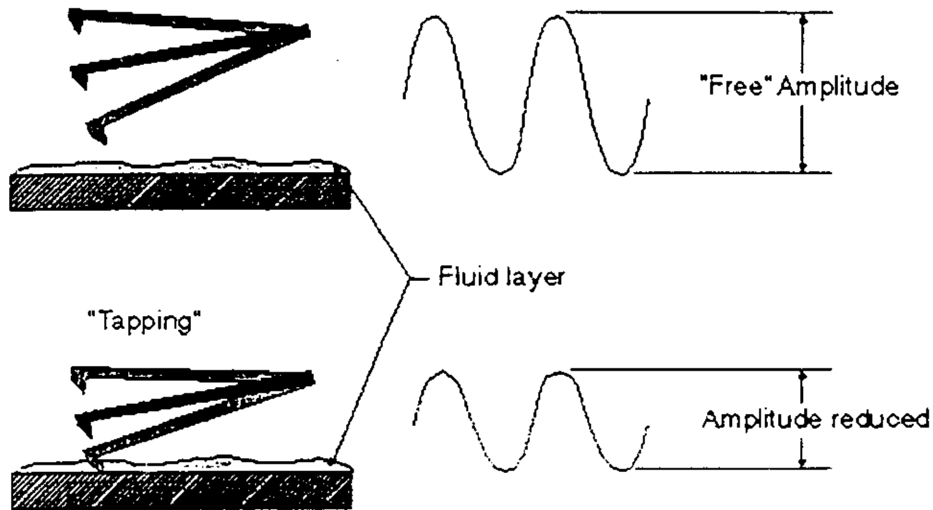

<u>Oscillation amplitude</u> ≅ 20 ÷ 100 nm

⇒ the tip "taps" the sample at each oscillation

a feedback loop can control oscillation amplitude

fig. 12

FORCE-DISTANCE CURVES

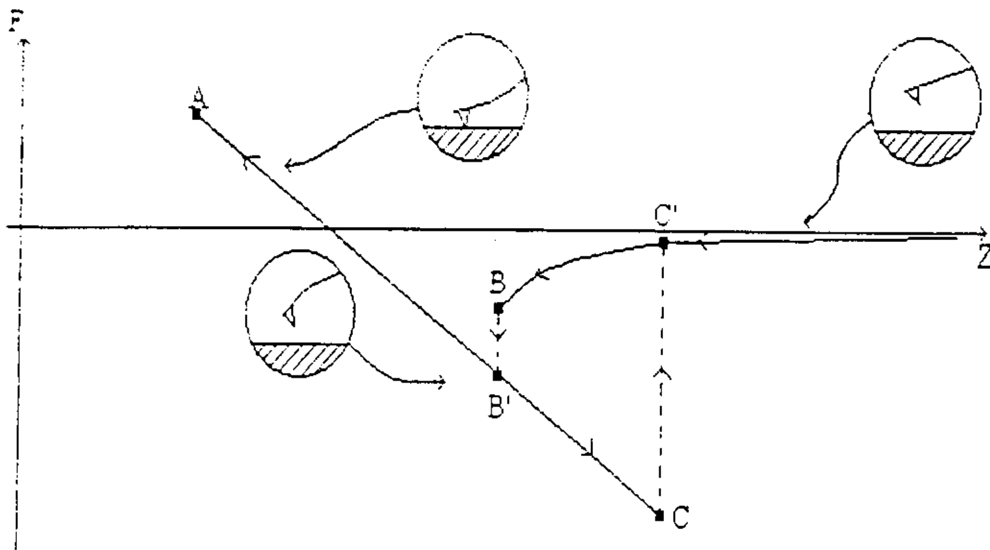

contact line	jump-to-contact	jump-off-contact
$Z=(1+k_l/k_c)\Delta s_l$	(van der Waals force between a sphere and a plane) $F_{attr} = -\frac{AR}{6D^2}$	$F_{ad} = -4\pi\rho\sqrt{\gamma_p\gamma_c}$
⇓ **compliance** ⇓ **elastic constant**	⇓ **attractive forces** ⇓ **Hamaker constant**	⇓ **adhesion** ⇓ **surface energies**

fig. 13

MICA in AIR

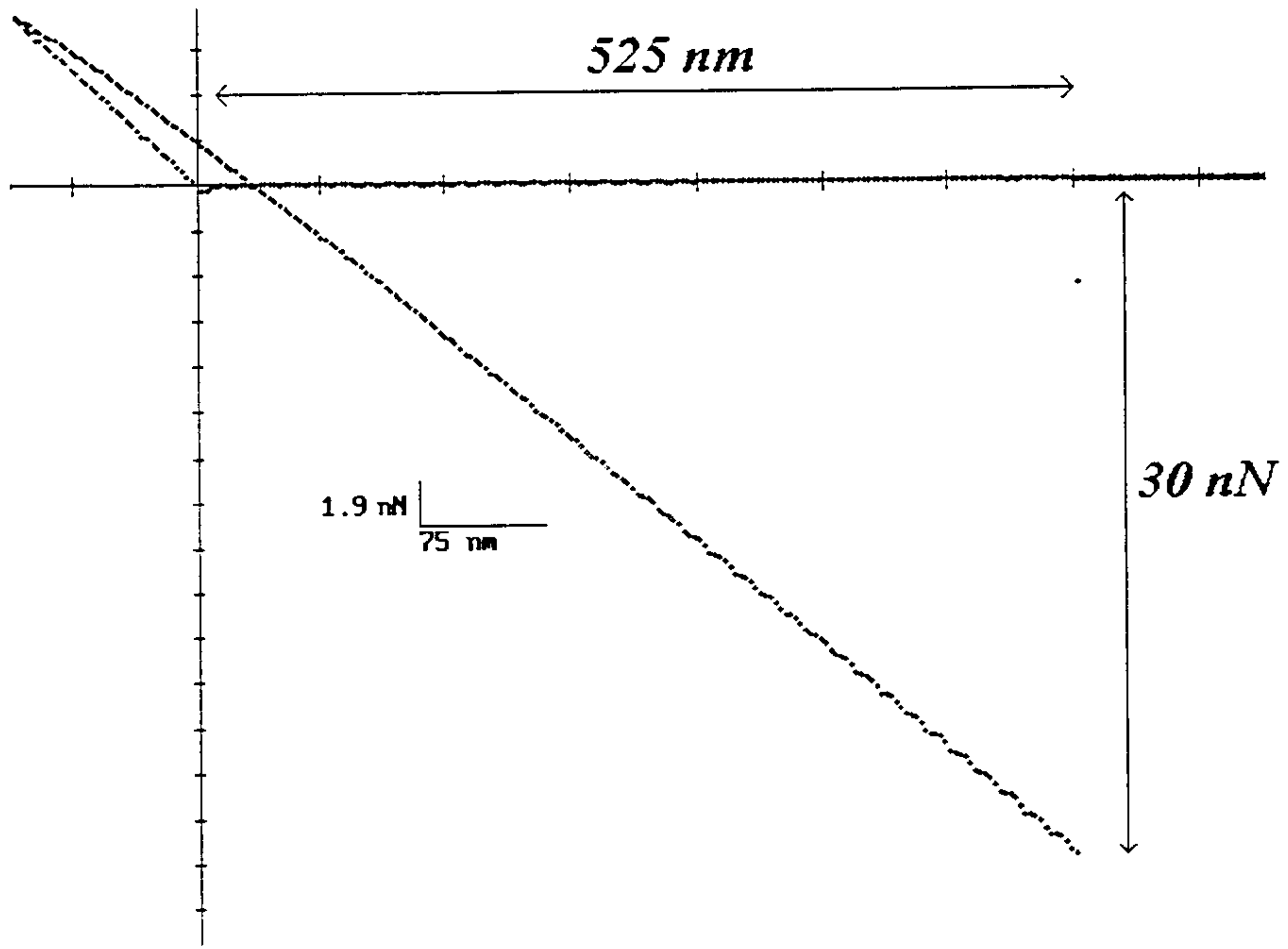

fig. 14

MICA in WATER

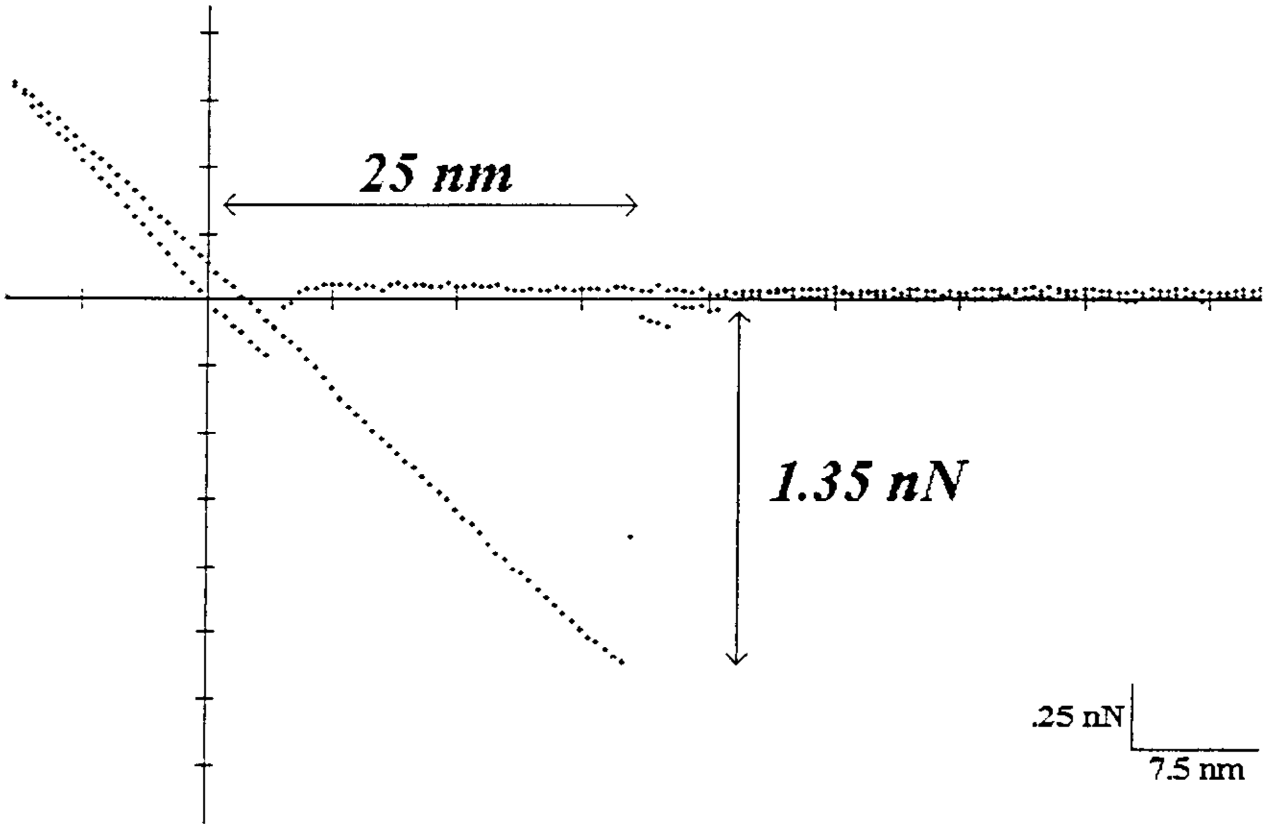

fig. 15

MICA in FORMAMIDE

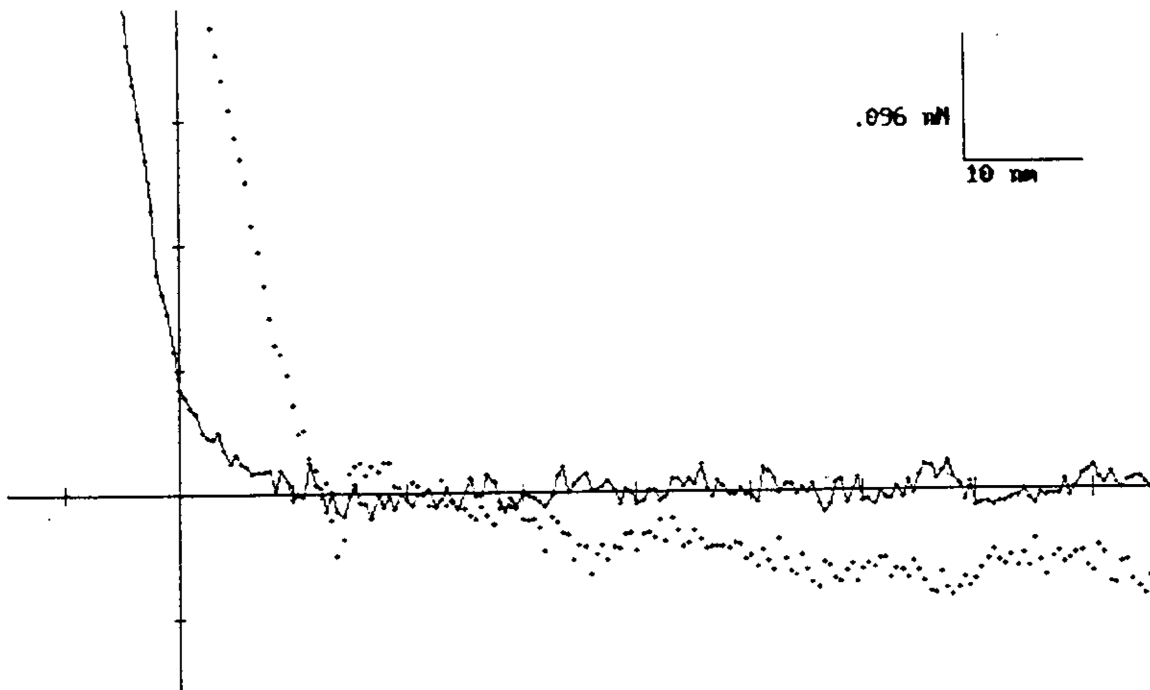

⇒REPULSIVE VAN DER WAALS (≅ 0.1 nN)

fig. 16

DOUBLE-LAYER FORCE

$$F = \frac{2\pi R}{\varepsilon\varepsilon_0\kappa}\left[\left(\sigma_T^2 + \sigma_S^2\right)e^{-2\kappa D} + 2\sigma_T\sigma_S e^{-\kappa D}\right]$$

Debye constant

$$\kappa = \sqrt{\sum_i \frac{\rho_{\infty i} e^2 z_i^2}{\varepsilon\varepsilon_0 kT}}$$

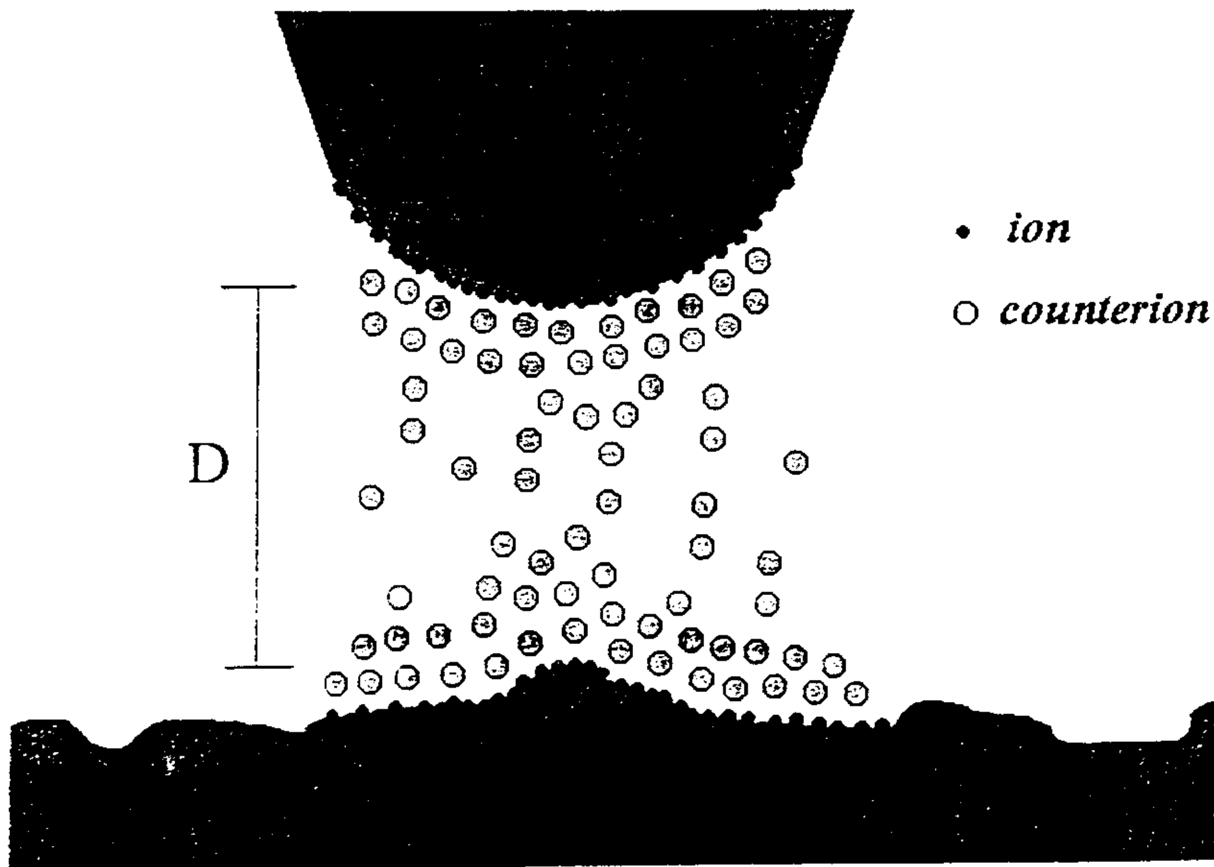

fig. 17

MICA in KCl SOLUTIONS

(approach curves)

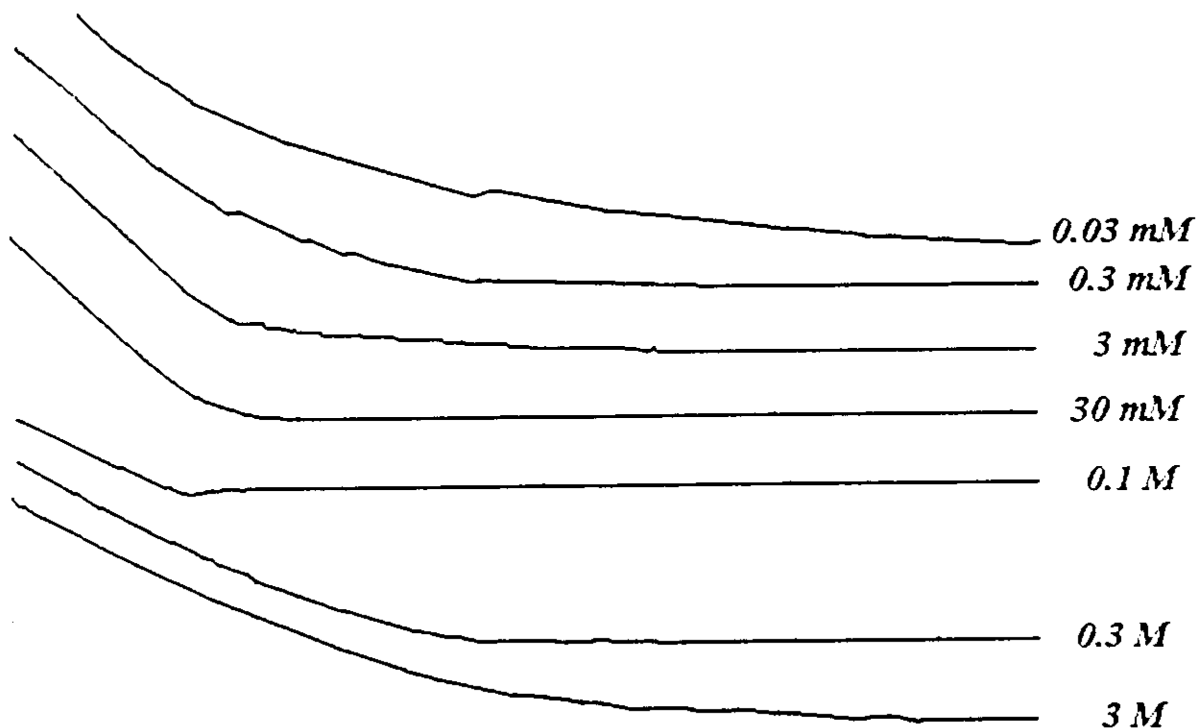

KCl<0.1 M

DOUBLE-LAYER
inversely proportional to the concentration

KCl=0.1 M

NO DOUBLE-LAYER

KCl>0.1 M

HYDRATION FORCE

fig. 18

MICA in $MgCl_2$ SOLUTIONS

(approach curves)

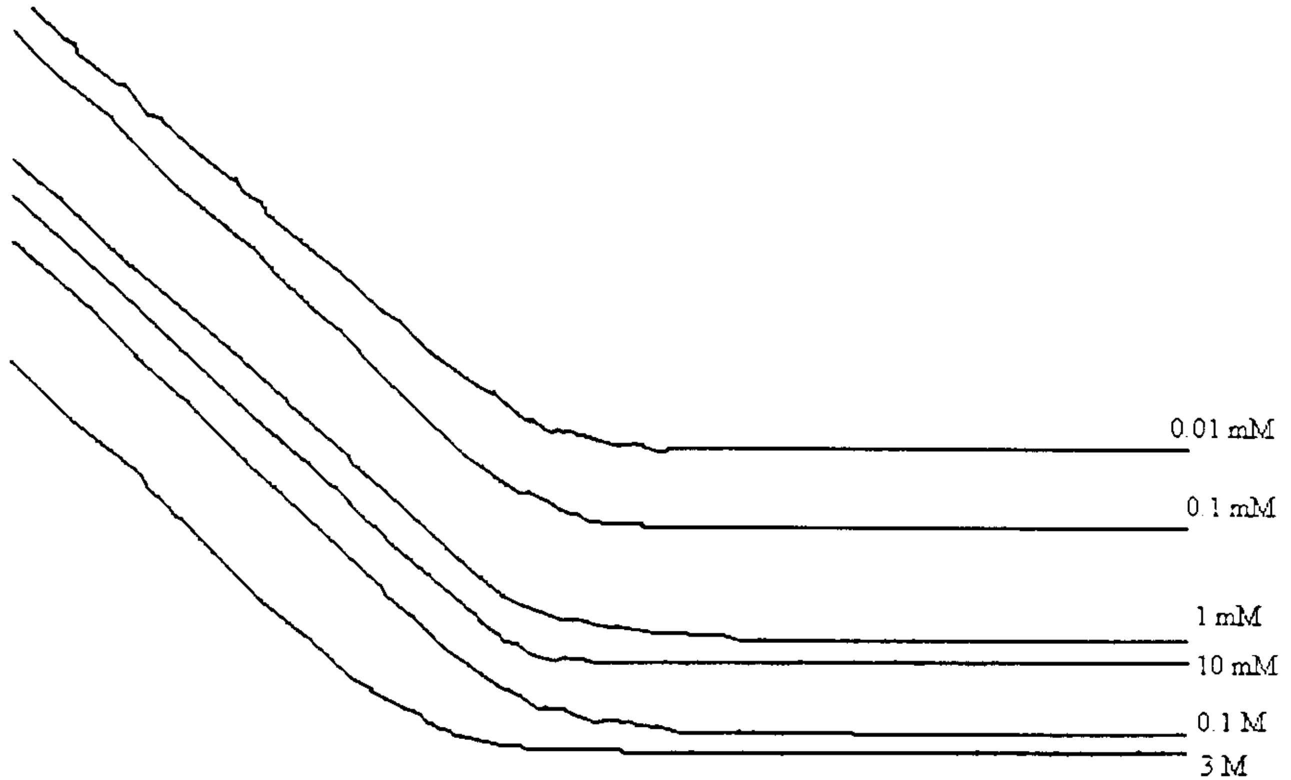

$MgCl_2$<30 mM

DOUBLE-LAYER
inversely proportional to the concentration

$MgCl_2$>0.1 M

HYDRATION FORCE

fig. 19

STEARIC ACID
in solution with different pH

(approach curves)

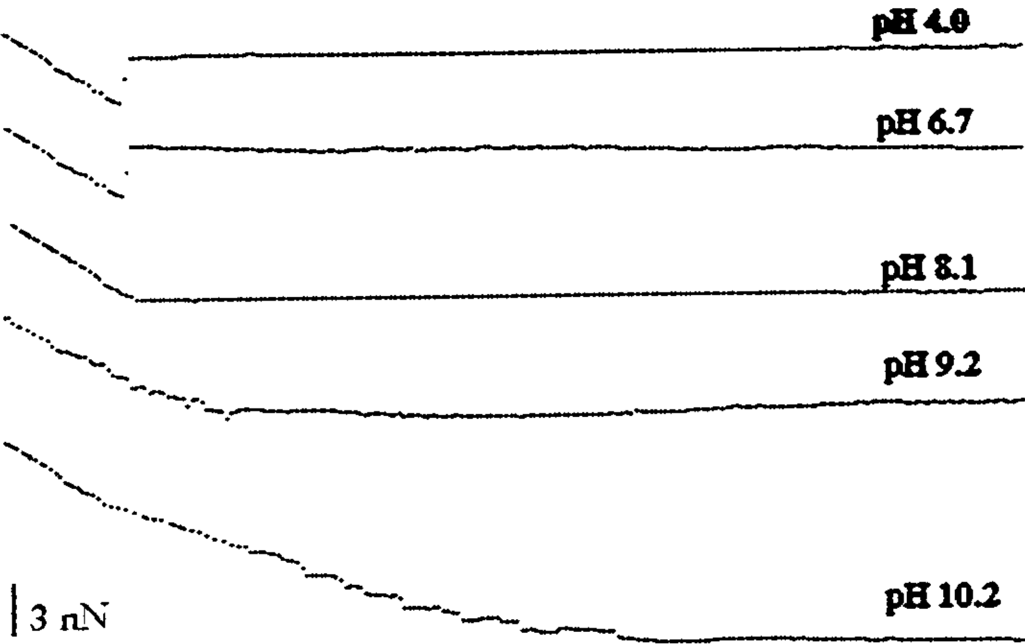

pH<8

uncharged sample ⇒ VAN DER WAALS

pH≅8

VAN DER WAALS ≅ DOUBLE-LAYER

pH>8

charged sample ⇒ DOUBLE-LAYER

fig. 20

HYDROPHOBIC FORCE

(withdrawal curves)

-Si_3N_4 tip on Au in water

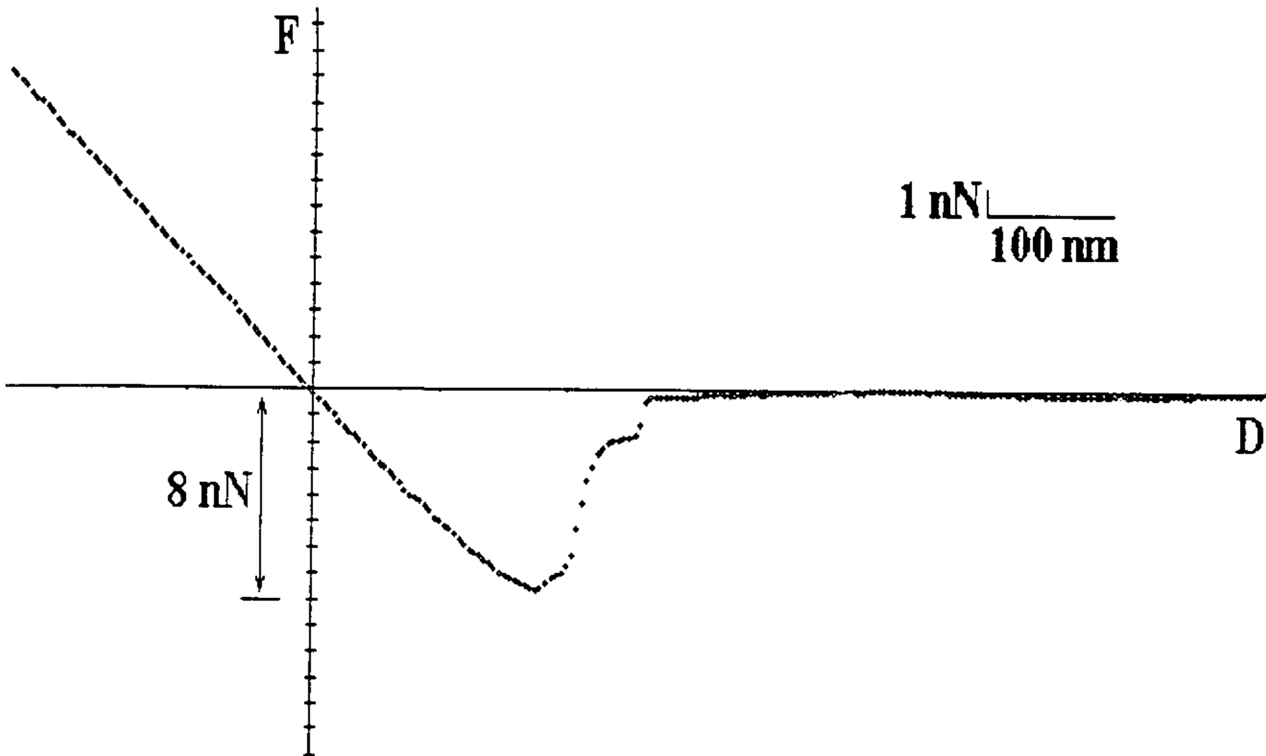

-Au tip on Au in water

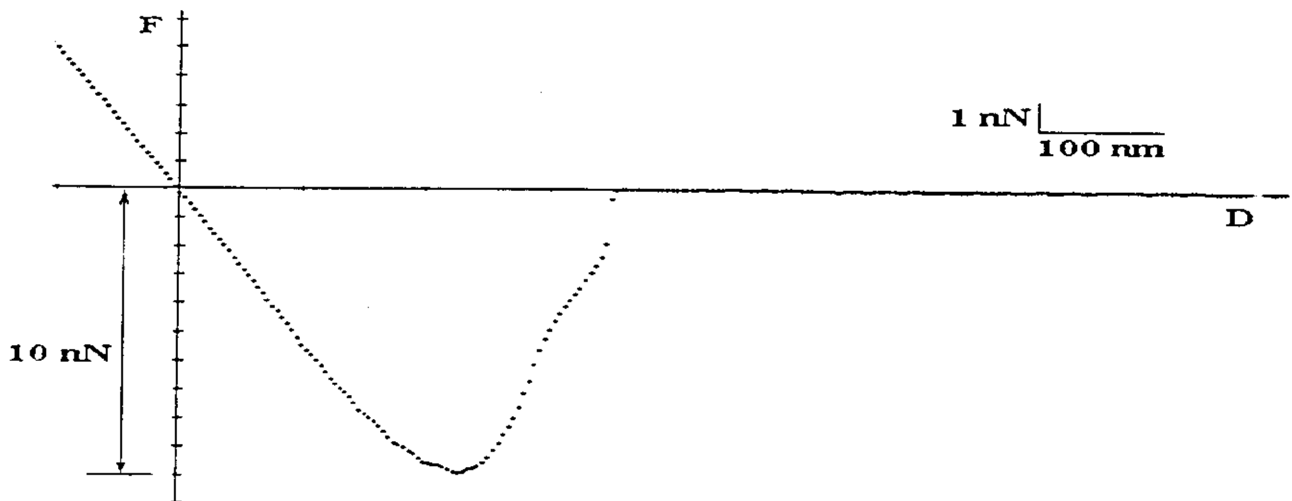

fig. 21

STEARIC ACID bridging forces

(withdrawal curve)

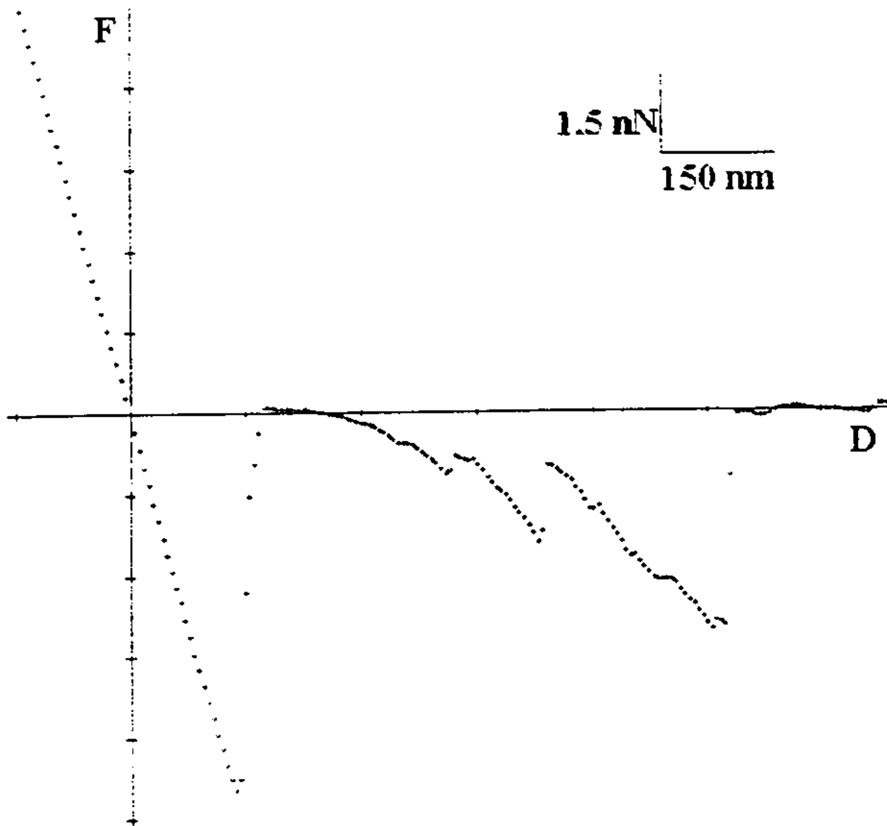

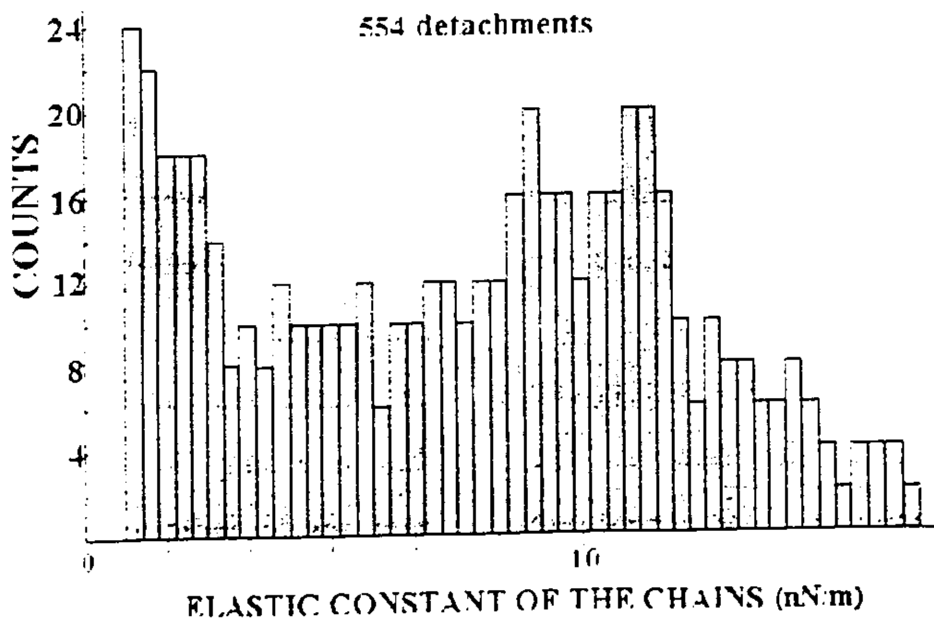

fig. 22

SOLVATION FORCE

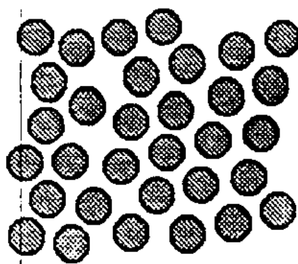

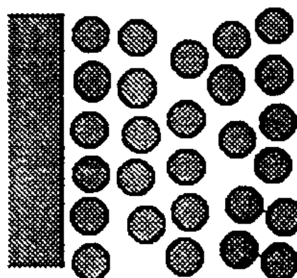

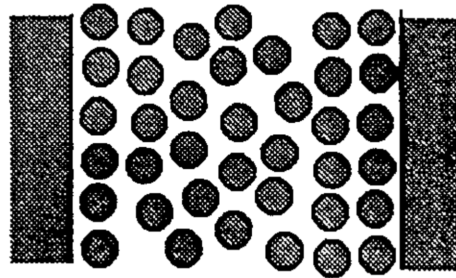

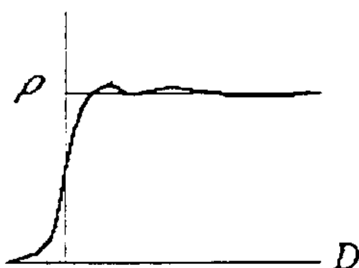

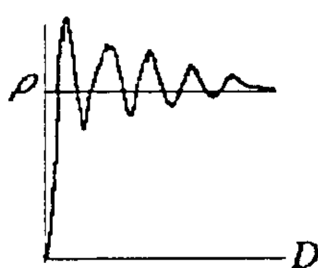

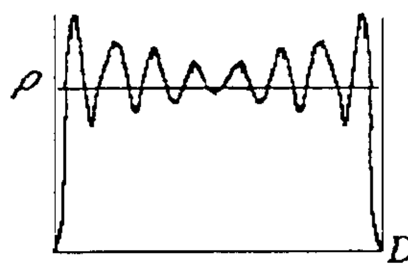

GRAPHITE IN OMCTS

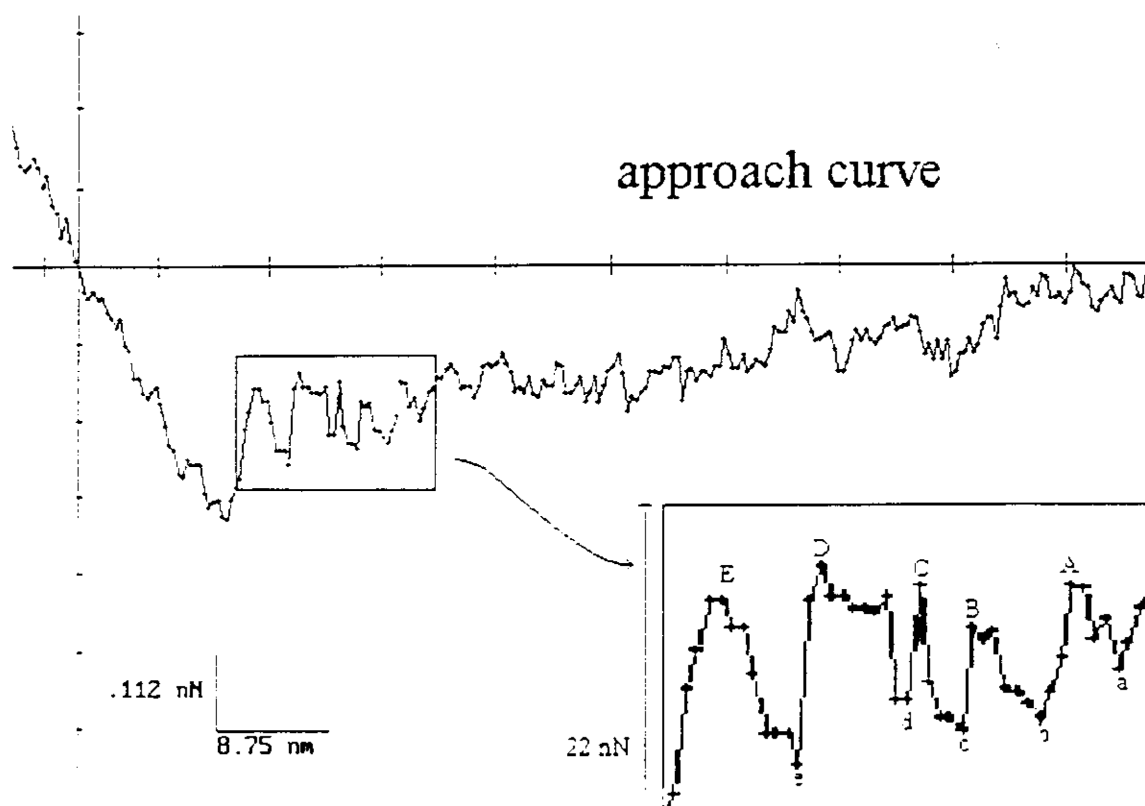

fig. 23

Origine des forces spécifiques

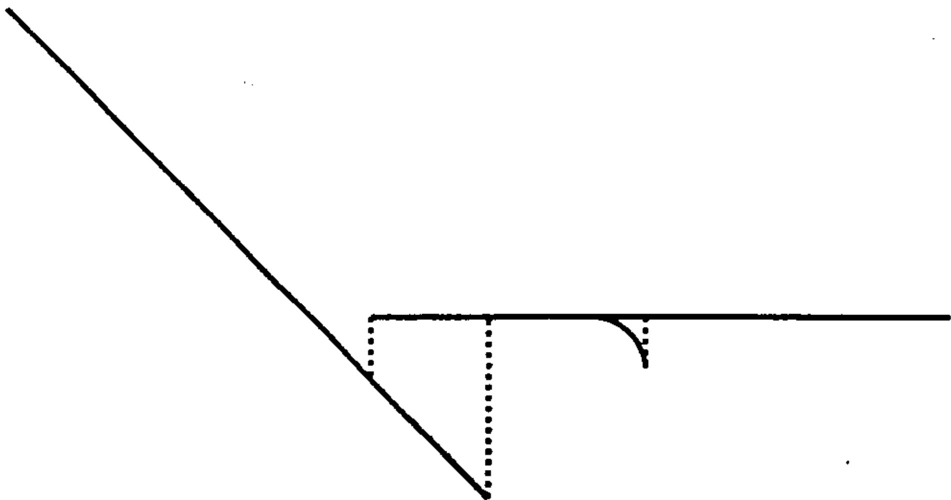

SPECIFIC FORCES

FUNCTIONALIZED TIP on OBP

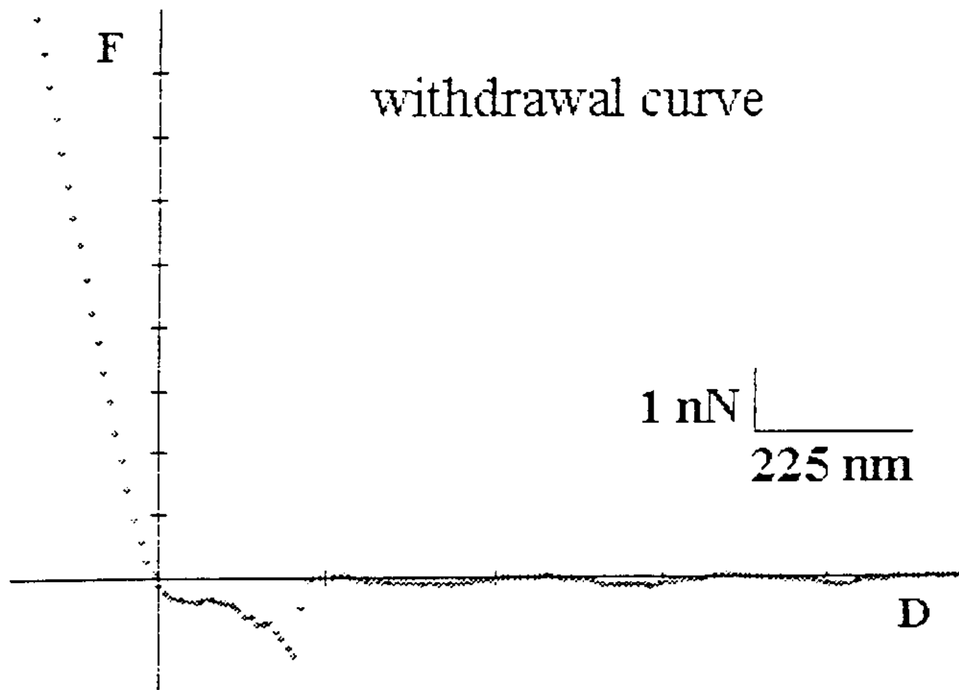

fig. 25

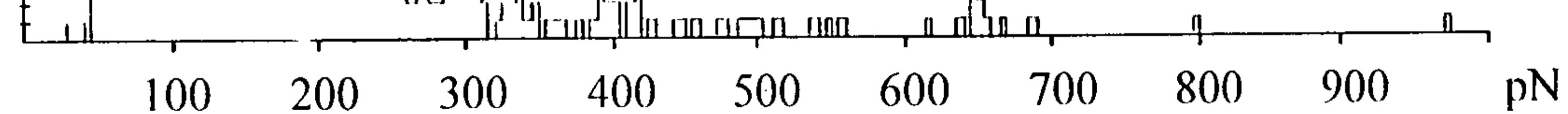
1099
0
1099 forces spécifiques/4096 courbes F-D
Temps de contact: 1500 ms, 500 ms, 250 ms, 125 ms
100
200
300
400
500
600
700
800
900
pN

FITC on SILICON

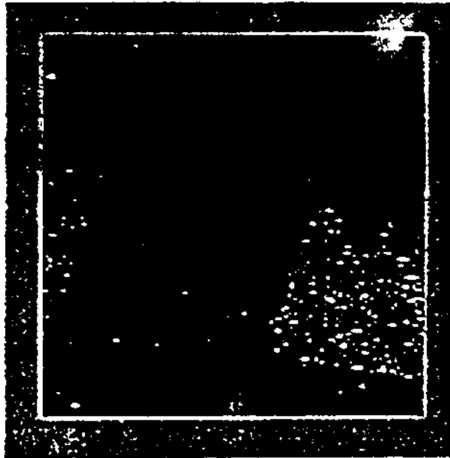

topography

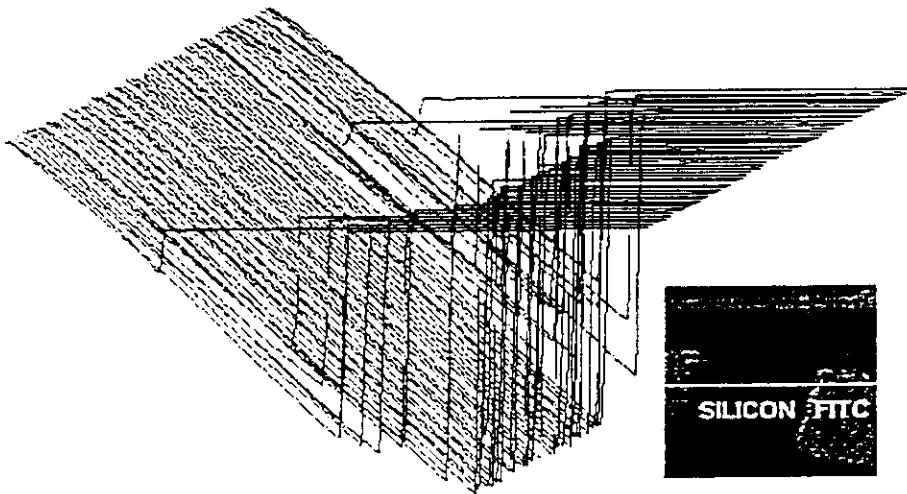

withdrawal force-distance curves on a line

fig. 27

FITC IN AIR

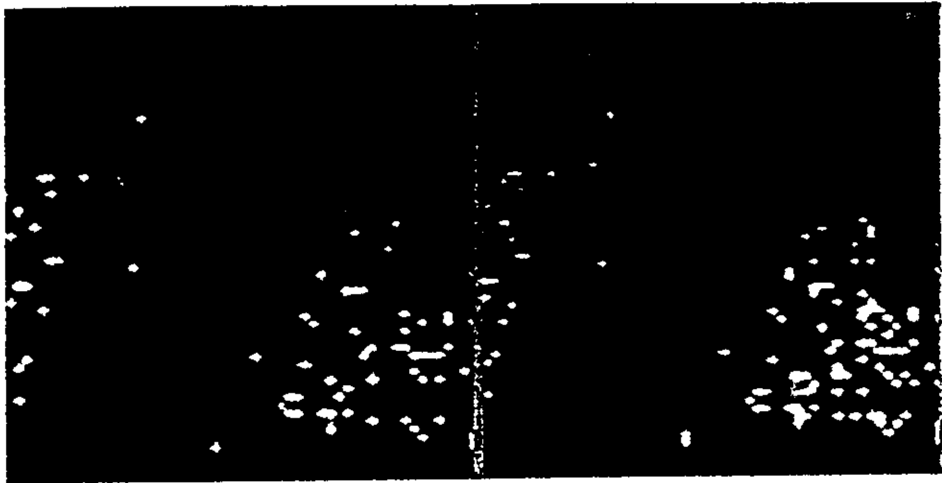

250 nm   300 nm

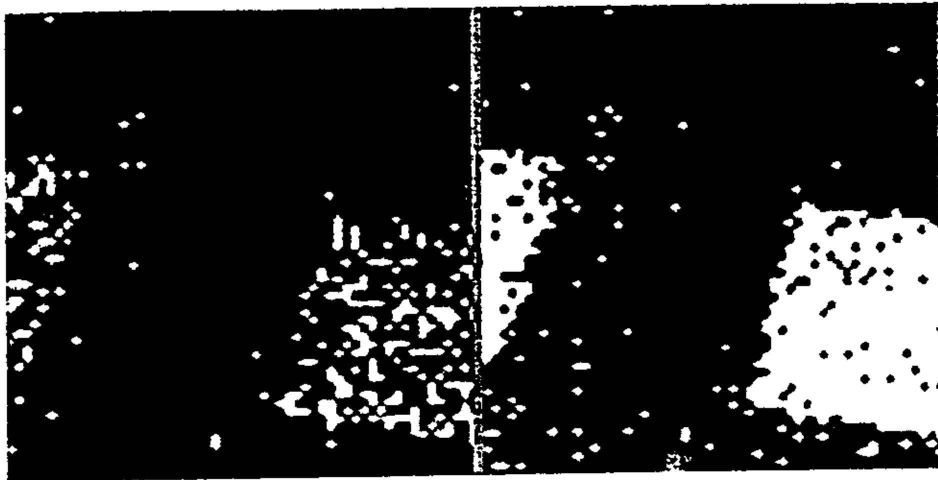

350 nm   440 nm

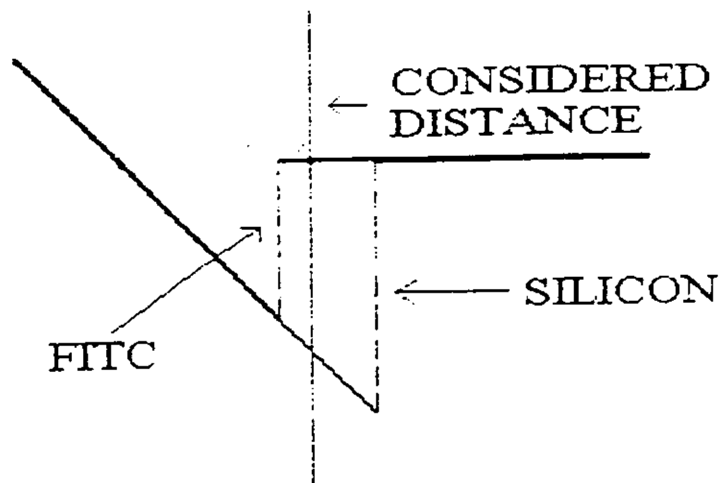

fig. 28

FITC IN AIR

COMPLIANCE

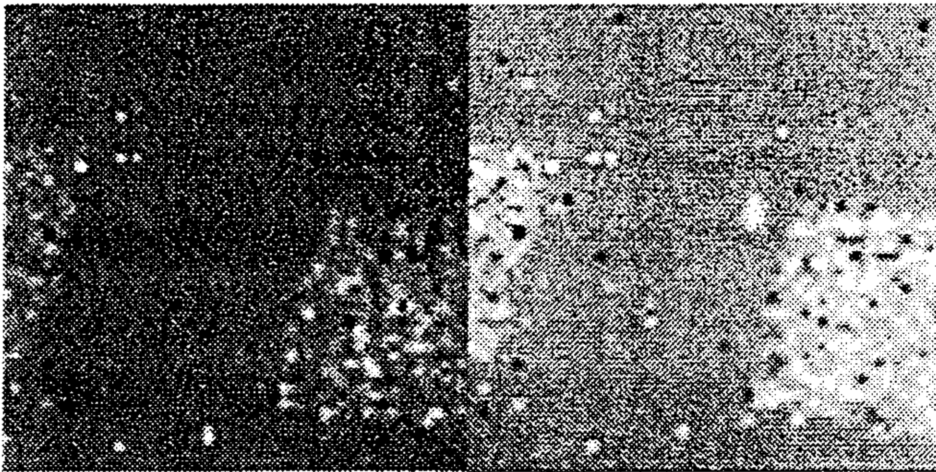

approach withdrawal

fig.29

MAPS

FITC IN AIR

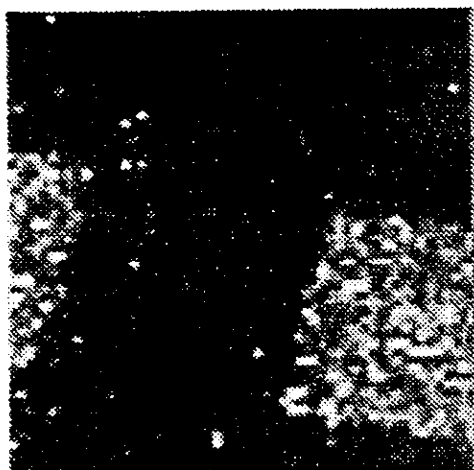

Jump off Contact Force

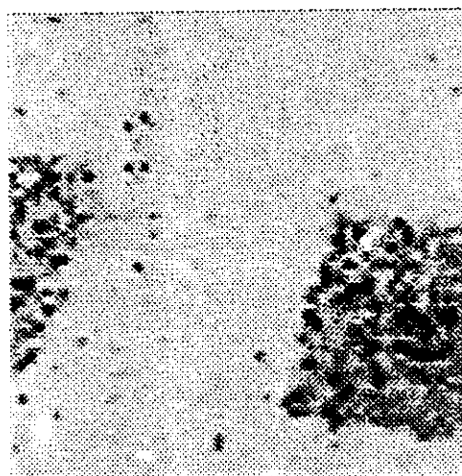

Jump off Contact Distance

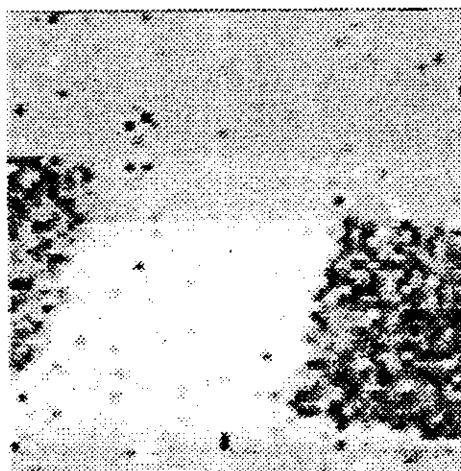

Adhesion

fig. 30

-Peroxidase in water

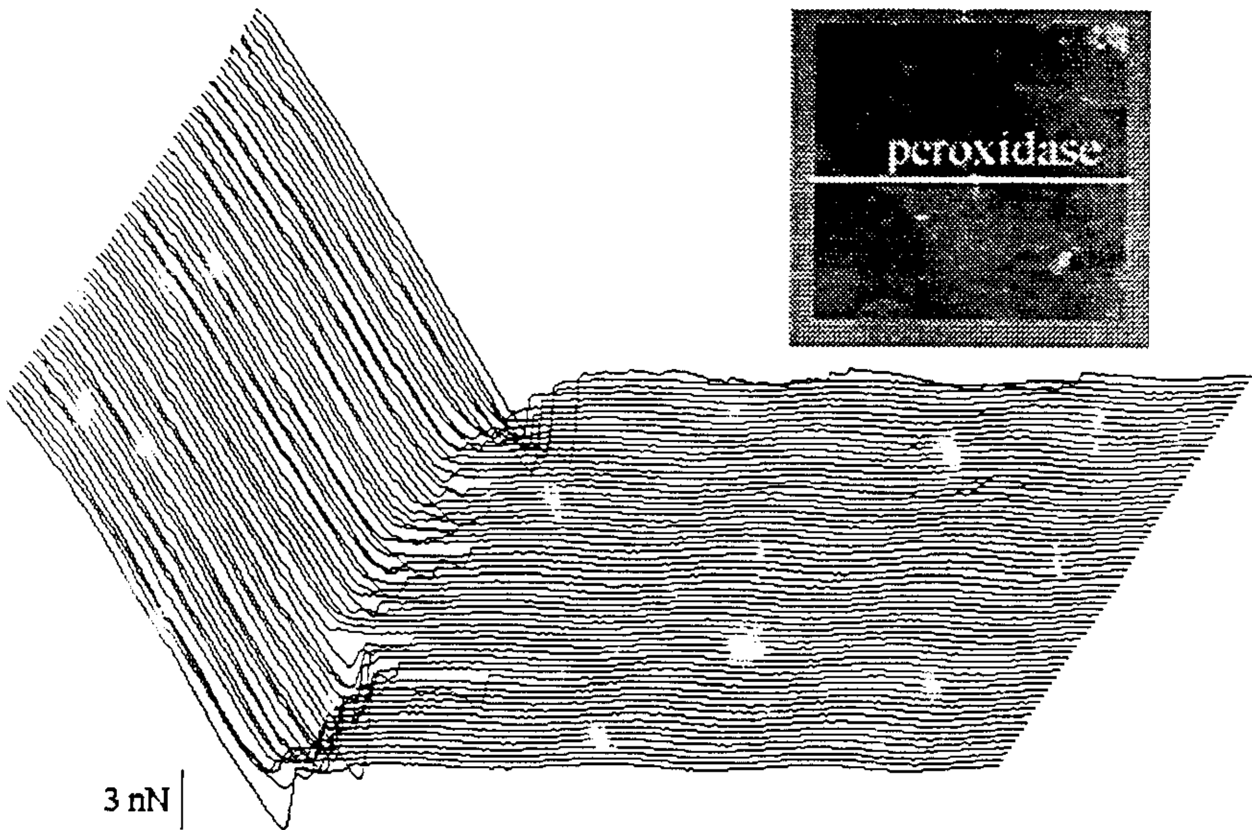

fig. 31

TRIPSIN IN WATER

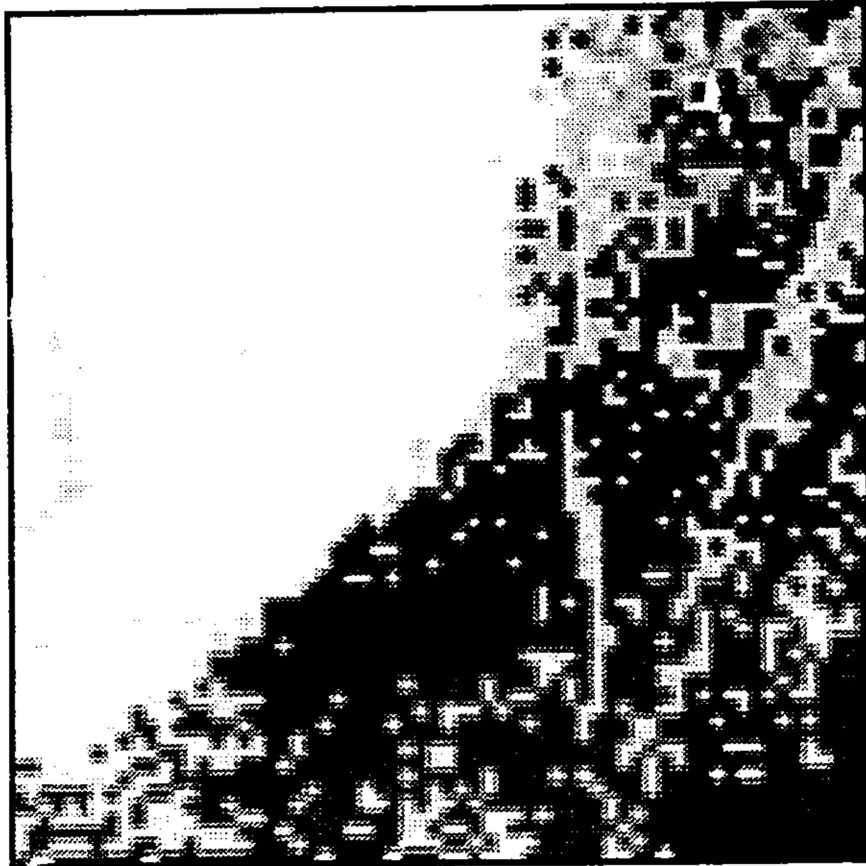

ADHESION MAP

fig. 32

REFERENCES

— a comprehensive review on AFM:

Sarid D., *Scanning Force Microscopy*, Oxford University Press, Oxford, 1991.

— on AFM:

Binnig G., Quate C.F., Gerber Ch., *Phys. Rev. Lett.*, **56**, p.930, 1986.

— on AFM cantilevers:

Sader J.E., White L., *J. Appl. Phys.*, **74**, p.1, 1993.
Tortonese M., *IEEE Engineering in Medicine and Biology*, **16**, p.28, 1996.

— on methods to detect cantilever deflections:

(tunneling)
Heinzelmann H. et al., *J. Vac. Sci. Technol.A*, **6**, p.275, 1988.
(inteferometric)
Mate C.M., Lorenz M.R., Novotny V.J., *J. Chem. Phys.*, **26**, p.1225, 1989.
(optical lever)
Meyer G., Amer N.M., *Appl. Phys. Lett.*, **53**, p.1045, 1988.
(noise)
Allegrini M. et al., *Ultramicroscopy*, **42-44**, p. 371, 1992

— on piezoelectric ceramics

Taylor M.E., *Rev. Sci., Instrum.*, **64**, p.154, 1993.
Waanders J.W., *Piezoelectric ceramics*, Philips, Eindhoven,1991.

— on non-contact mode

Anselmetti D. et al., *Nanotechnology*, **5**, p.87, 1994.

— on tapping mode

Hansma P. K. et al., *Appl. Phys. Lett.*, **64**, p.1738, 1994.
Putman C. A. J. et al., *Appl. Phys. Lett.*, **64**, p.2454, 1994.
Zhong Q., Inniss D., Kjoller K., Elings V.B., *Surf. Sci Letters*, **290**, L688, 1993.

— on friction

Hamada E., Kaneko R., *Ultramicroscopy*, **42-44**, p.184, 1992.
Meyer E. et al., *Phys. Rev. Lett.*, **69**, 1992.

—on surface forces

Hartmann U. in *Scanning Tunneling Microscopy III*, Springer Verlag, 1993.
Israelachvili J.N., *Intermolecular and surface forces*, 2nd ed., p.55, Academic Press, London, 1992.

— on force-distance curves

Aimè J.P. et al., *J. Appl. Phys.*, **76**, p.754, 1994.
Burnham N.A., Colton R.J., *J. Vac. Sci. Technol. A*, **7**, p.2096, 1989.
Burnham N.A, Dominguez D.D., Mowery R.L., Colton R.J., *Phys. Rev. Lett.*, **64**, p.1931, 1990.
Butt H.J., *Biophys. J.*, **60**, p.777, 1991.
Butt H.J., *Biophys. J.*, **60**, p.1438, 1991.
Cappella B. et al., *IEEE Engineering in medicine and biology*, **16**, p. 58, 1997
Hao H.W., Barò A.M., Saenz J.J., *J. Vac. Sci. Technol. B*, **9**, p.1323, 1991.
Hartmann U., *Phys. Rev. B*, **43**, p.2404, 1991.
Hoh J.H. et al., *J. Am. Chem. Soc.*, **114**, p.4917, 1992
Ishino T., Hieda H., Tanaka K., Gemma N., *Jpn. J. Appl. Phys.*, **33**, p.4718, 1994.
Landman U., Luedtke W.D., Burnham N.A., Colton R.J., *Science*, **248**, p.454, 1990.
Mate C.M., Lorenz M.R., Novotny V.J., *J. Chem. Phys*, **90**, p.7550, 1990.
Meyer E. et al., *J. of Microscopy*, **152**, p.269, 1988.
O'Shea S.J., Welland M.E., Rayment T., *Appl. Phys. Lett*, **60**, p.2356, 1992.
Weisenhorn A.L., Maivald P., Butt H.J., Hansma P.K., *Phys. Rev. B*, **45**, p.11226, 1992.
Ishino T.. Hieda H., Tanaka K., Gemma N.. *Jpn. J. Appl. Phys.*, **33**, p.4718, 1994.

— on force-distance curves mapping

Baselt D.R., Baldeschwieler J.D., *J. Appl. Phys.*, **76**, p.33, 1994.
Cappella B. et al., *Nanotechnology*, **8**, p. 82, 1997.
Joyce S., Houston J.E., Michalske T.A., *Appl. Phys. Lett.*, **60**, p.1175, 1992.
Radmacher M. et al., *Biophys. J.*, **66**, p.2159, 1994.
van der Werf K.O., Putman C.A., de Grooth B.G., Greve J., *Appl. Phys. Lett.*, **65**, p.1195, 1994.

— on specific forces

Florin E.L., Moy V.T., Gaub H.E., *Science,* **264**, p.415, 1994.
Lee G.U., Chrisey L.A., Colton R.J., *Science*, **266**, p.771, 1994.
Moy V.T., Florin E.L., Gaub H.E., *Science,* **266**, p.257, 1994.
Nakagawa T., Ogawa K., Kurumizawa T., Ozaki S., *Jpn. J. Appl. Phys*, **32**, p.L294, 1993.

Overview:

Technology of proximal Probe Lithography, edited by C.R.K. Marrian (SPIE Optical Engeneering Press, Bellingham, WA, 1993) and reference therein.

The AFM as an *e-beam writer*:

A. Majumdar *et al.*, *Appl. Phys. Lett.* **61**, 2293 (1992).

Polymers modification:

E. Boschung, M. Heuberger, and G. Dietler, *Appl. Phys. Lett.* **64**(26), 3565 (1994).

X. Jin and W.N. Unertl, *Appl. Phys. Lett.* **61**(6), 657 (1992);

T.A. Jung, A. Moser, H.J. Hug, D. Brodbeck, R. Hofer, H.R. Hidber, and U.D. Schwarz, *Ultramicroscopy* **42-44**, 1446 (1992);

Metals modification:

H. Gobel and P. Von Blanckenhagen, *J. Vac. Sci. Technol. B* **13**(3), 1247 (1995);

T. Sumonogi, T. Endo, and K. Kuwahara, *J. Vac. Sci. Technol. B* **13**(3), 1257 (1995).

Semiconductors modification:

R. Magno and B.R. Bennett, *Appl. Phys. Lett.* **70**, 1855 (1997).

Nanofabrication on a PMMA *multilayer*:

! .L. Sohn and R.L. Willet, *Appl. Phys. Lett.* **67**(11), 1552 (1995).

Nanofabrication on UV-fotoresist:

M. Wendel, S. Kühn, H. Lorenz, and J.P. Kotthaus, *Appl. Phys. Lett.* **65**(14), 1775 (1994).

Other:

Y. Okada *et. al.*, J. of Appl. Phys. **83**, 1844 (1998);

E.S. Snow and P.M. Campbell, Appl. Phys. Lett. **64**, 1932 (1994).

E.S. Snow and P.M. Campbell, Appl. Phys. Lett. **69**, 269 (1996).

H. Sugimura *et al.*, Appl. Phys. Lett. **63**, 1288 (1993);